NITRIC OXIDE-INDUCED MODIFICATION OF PROTEIN THIOLATE CLUSTERS AS DETERMINED BY SPECTRAL FLUORESCENCE RESONANCE ENERGY TRANSFER IN LIVE ENDOTHELIAL CELLS

by

Karanee Leelavanichkul

BS, Washington University in Saint Louis, 2001

Submitted to the Graduate Faculty of

School of Engineering in partial fulfillment

of the requirements for the degree of

Master of Science in Bioengineering

University of Pittsburgh

2005

UNIVERSITY OF PITTSBURGH

SCHOOL OF ENGINEERING

This thesis was presented

by

Karanee Leelavanichkul

It was defended on

February 24, 2005

and approved by

Dr. Partha Roy, Assistant Professor, Department of Bioengineering

Dr. Claudette M. St. Croix, Assistant Professor, Department of Environmental and Occupational Health

Thesis Advisor: Dr. Bruce R. Pitt, Professor and Chairman of the Department of Environmental and Occupational Health

ABSTRACT

NITRIC OXIDE-INDUCED MODIFICATION OF PROTEIN THIOLATE CLUSTERS AS DETERMINED BY SPECTRAL FLUORESCENCE RESONANCE ENERGY TRANSFER IN LIVE ENDOTHELIAL CELLS

Karanee Leelavanichkul, MS

University of Pittsburgh, 2005

Low-molecular-weight S-nitrosothiols are found in many tissues and recognized to affect a diverse array of signaling pathways via decomposition to ·NO or exchange of their −NO function with thiol containing proteins (transnitrosation). We used spectral laser scanning confocal imaging to visualize the effects of D- and L- stereoisomers of S-nitrosocysteine ethyl ester (SNCEE) on fluorescence resonance energy transfer (FRET)-based reporters that are targets for the following NO-related modifications: (a) S-nitrosation, via the cysteine-rich, metal binding protein, metallothionein (FRET-MT); and (b) nitrosyl-heme-Fe- guanosine 3′,5′-cyclic monophosphate (cygnet-2) in live cells. Conformational changes consistent with S-nitrosation of FRET-MT were specific to L-SNCEE. In addition, they were reversed by dithiothreitol (DTT) but unaffected by exogenous oxyhemoglobin (HbO_2). In contrast, D- and L-SNCEE had comparable effects on cygnet-2, likely via activation of soluble guanylyl cyclase (sGC) by ·NO as they were sensitive to the sGC inhibitor, 1H-[1,2,4]-oxadiazolo[4,3-α] quinoxalin-1 (ODQ)

and exogenous oxyhemoglobin. These data demonstrate the utility of spectral laser scanning confocal imaging in revealing subtle aspects of NO signal transduction in live cells. Stereoselective transnitrosation of metallothionein (MT) suggests that the structure of L-SNCEE confers access to critical cysteine(s) in the protein. Such stereo-selectivity underscores the specificity of post-translational modification as a component of NO signaling.

TABLE OF CONTENTS

LIST OF FIGURES

LIST OF ABBREVIATIONS

cGMP	=	guanosine 3′,5′-cyclic monophosphate
Cygnet-2	=	cyclic GMP indicator using energy transfer
DTT	=	dithiothreitol
ECFP	=	enhanced cyan fluorescent protein
EYFP	=	enhanced yellow fluorescent protein
FRET	=	fluorescence resonance energy transfer
GFP	=	green fluorescent protein
HbO_2	=	oxyhemoglobin
LSCM	=	laser scanning confocal microscopy
MT	=	metallothionein
NO	=	nitric oxide
NOS	=	nitric oxide synthase
ODQ	=	1H-[1,2,4]-oxadiazolo[4,3-α] quinoxalin-1
PKG	=	cGMP-dependent protein kinase
sGC	=	soluble guanylyl cyclase
SNCEE	=	S-nitrosocysteine ethyl ester
SNO	=	S-nitrosothiol
SPAEC	=	sheep pulmonary artery endothelial cells

ACKNOWLEDGEMENTS

None of the work presented would have been possible without the help, support and encouragement of following people.

First I want to especially thank Dr. Bruce Pitt, my advisor for the opportunity to work for him and his confidence and willingness to help me achieve my goals. I am also grateful to him for providing the financial and academic support that has benefit me in my years of study.

I would like to express my gratitude to Dr. Claudette St. Croix, my mentor, for her guidance and many helpful insights giving throughout my graduate studies. I owe much for her time explaining every concept of this work, and her dedication and patience to the entire thesis process.

I would like to thank Dr. Partha Roy for serving on my examining committee and his helpful comments on the work. I'm also thankful to the Pitt lab members, especially Karla Wasserloos, Molly Stitt, and Xianghong Liu for teaching everything I need to know to survive in the lab and for making the lab a more enjoyable workplace. Special thanks go out to Dr. Zilue Tang, who always encourages me to stay focus and Dr. Simon Watkins, director of the Center for Biological Imaging for his hospitality and help with microscopy.

Finally, I would like to thank my friends and family, especially my father, my mother and my grandfather without their endless love and support I would have never made it this far, and many thanks to my brothers and sisters who were always there to tell me a funny story and made me laugh.

1.0 OVERVIEW

S-nitrosothiols are adducts of nitric oxide (·NO) and thiol-containing compounds that are found in many mammalian tissues and are suggested to affect a diverse array of physiological functions, including signal transduction and immune responses [1]. The bioactivities of low-molecular-weight S-nitrosothiols may be mediated either by their decomposition to ·NO or by direct exchange of their NO function with thiol-containing proteins (transnitrosation) [2].

Detection of interactions between target proteins and nitrogen oxide species *in vivo* typically requires disruptive biochemical techniques that preclude or limit temporal–spatial information. Although significant technological advancements have promoted an increased reliance on the use of high-performance multimodal optical imaging tools to visualize cellular processes in biological systems, the imaging of NO-based signaling events remains especially challenging. One successful example is the use of spatial–spectral electron paramagnetic resonance imaging, in combination with isotope tracer methods, to map nitrite-derived NO production in the isolated ischemic rat heart [3]. More recently, the fluorescent indicator 4,5-diaminofluorescein [4, 5] has been widely used for detection and imaging of ·NO but is hampered by concerns regarding its selectivity [6, 7], sensitivity [6], and interactions with divalent cations [8].

The development of genetically encoded probes based on green fluorescent protein from the Pacific jellyfish, *aequorea victoria*, has been instrumental in advancing the use of fluorescent

resonance energy transfer (FRET) technologies to investigate molecular interactions in living systems. FRET is a quantum mechanical process whereby two fluorophores (i.e. donor and acceptor pair) that are closely apposed (<10 nm) transfer photon energy in a non-radiative fashion. The FRET effect decreases with the sixth power of the distance between the donor and acceptor fluorophores. This relationship allows the use of FRET to measure physical interactions among proteins, or among domains within a single protein.

The validity of FRET-based approaches to studying intracellular signaling pathways in live cells has been demonstrated using fluorescent reporter molecules for calcium [9], guanosine 3′,5′-cyclic monophosphate (cGMP) [10], 3′,5′-cyclic adenosine monophosphate (cAMP) [11], and tyrosine kinase activity [12], among others. Our recent efforts utilizing this methodology to elucidate the role of metallothioneins (MT) in NO signaling [13, 14] suggest that FRET is suitable for detection of posttranslational protein modifications caused by nitric oxide-related species.

Most methods for detecting FRET between a donor and an acceptor molecule with overlapping excitation and emission spectra require the use of narrow detection bands and automatic switching of optical filters to differentiate between emissions, along with complex mathematical corrections to account for crosstalk between channels. Recent advances in detector technology, however, enable the resolution of fluorescent images providing full spectral information for each voxel of the image without switching of optical filters. Furthermore, using calibration spectra, it is possible to unambiguously separate the cross-talk between overlapping cyan and yellow emissions. The use of this method allows the detection of small, but potentially biologically meaningful, changes in FRET that are common with genetically encoded reporters

and are extremely difficult to resolve reliably using more traditional methods relying on bandpass filters.

Accordingly, the specific aims of the project were to:

1) detect, and distinguish between, NO-related signaling events that are due to protein S-nitrosation, or the formation of nitrosyl-heme-Fe- complexes in living cells using FRET-based reporters based on the cysteine-rich, metal binding protein, metallothionein (FRET-MT); and guanosine 3′,5′-cyclic monophosphate (cygnet-2), respectively.

2) investigate the utility of spectral laser scanning confocal imaging in revealing subtle aspects of NO signal transduction in live cells.

2.0 BACKGROUND

2.1 NITRIC OXIDE (NO)

Nitric oxide (NO) is a hydrophobic diatomic gas that is synthesized in many different cells type and tissues. NO has an extremely short half-life (<5 s) *in vivo* [15]. However, because of its high solubility in nonpolar solvents, it is readily diffusible and therefore has biological effects far from the site of production [15]. As an uncharged molecule with one unpaired electron, NO commonly reacts with other paramagnetic species (oxygen, O_2 or superoxide, $O_2^{\cdot -}$) or forms complexes with metal centers. The three main reactions of NO are nitration (addition of NO_2), nitrosation (addition of NO^+), and nitrosylation (addition of ·NO). The bioactivities of NO are largely mediated by nitroxyl (NO^-) or nitrosonium (NO^+). In aqueous solution, these chemical species have a half-life of less than 1 second but are stabilized in biological complexes with thiols (RS^-), and other targets and intermediates [16].

2.1.1 NO synthesis

Nitric oxide is generated from L-arginine in the presence of molecular oxygen and nicotinamide adenine dinucleotide phosphate (NADPH) and with the aid of other cofactors such as flavin mononucleotide (FMN), flavin adenine dinucleotide (FAD), tetrahydrobiopterin (H4B),

heme, and calcium (Ca^{2+})/calmodulin [17]. The reaction is catalyzed by the action of nitric oxide synthase (NOS) and yields the coproduct L-citrulline in addition to nitroxyl (HNO).

There are at least three distinct NOS isoforms. NOS I (neuronal NOS, nNOS) has a widespread distribution in the central and peripheral nervous system where it plays a role in neurotransmission, neural development, regeneration, synaptic plasticity and regulation of gene expression. The expression of NOS II (inducible NOS, iNOS) and synthesis of NO are induced by cytokines and lipopolysaccharide. Stimulation of NOS II may contribute in part to the NO-mediated fall in pulmonary vascular resistance (PVR) during shear stress-induced pulmonary vasodilation [18]. NOS III (endothelial NOS, eNOS) was first characterized in vascular endothelial cells but has subsequently been demonstrated in a number of non-endothelial cell types including hippocampal neurons, cardiomyocytes, and blood platelets. NOS III is subjected to expressional regulation by shear stress and exercise [19], endothelial cell proliferation [20], and hypoxia [21]. A number of agonists such as bradykinin, acetylcholine, serotonin and histamine activate NOS III by causing increases in intracellular free calcium.

The most important physiological stimulus for the continuous formation of NO in the endothelial cell layer is the shear stress generated by blood flow [19, 22, 23]. Though the precise shear stress sensor is unknown, it may involve conformational changes in caveolae at the luminal endothelial cell surface, causing dissociation of eNOS (NOS III) from caveolin and allowing activation by calmodulin and other effectors [24, 25]. The signal transduction pathway has not been delineated but appears to involve both Ca^{2+}-dependent and phosphorylation events [26, 27].

2.1.2 **NO signaling in physiologic systems** [28]

Among its many biological effects nitric oxide has been shown to play a central role in smooth muscle relaxation, blood vessel formation (angiogenesis), and inflammatory processes [29]. In the brain, NO acts as a neurotransmitter in the central and peripheral nervous systems and is important for controlling the release of other neurotransmitters like glutamate and acetylcholine [30]. NO has also been shown to be involved in regulating apoptosis in a number of cells types including neurons [31]. NO is produced by a number of inflammatory cells and has been shown to play a role in modulating immune responses. In particular the high concentrations of NO produced by cytokine-activated macrophages are toxic to target cells such as bacteria or tumor cells. NO production is induced, through the up-regulation of iNOS, by a number of factors involved in inflammation, including interleukins, interferon-gamma, TNF-alpha and LPS. [32]. NO also acts as a mediator of inflammatory processes by enhancing the effect of cyclooxygenases [33, 34]. NO-mediated cytotoxicity has been shown to kill cells by disrupting enzymes involved in the Kreb's cycle, DNA synthesis and mitochondrial function [35].

2.1.3 **Direct effects of NO** [36]

Once NO is synthesized, it rapidly diffuses and interacts with intracellular molecular sites within both generating and target cells. NO rapidly reacts with transition metals, which have stable oxidation states differing by one electron. Complexes of ferric iron (Fe^{3+}) with NO are called nitrosyl compounds which can also nitrosate (donate NO^{+}) thiol groups (-SH), while reducing the ion to the ferrous (Fe^{2+}) state (Equation 1).

$$RSH + [Fe^{3+} - NO \leftrightarrow Fe^{2+} - (NO^{+})] \rightarrow RSNO + Fe^{2+} + H^{+} \quad (1)$$

One of the best recognized targets for eNOS-derived NO is soluble guanylyl cyclase (sGC). sGC is a heterodimeric hemoprotein composed of α and β subunits which catalyzes the conversion of guanosine triphosphate (GTP) to cyclic guanosine monophosphate (cGMP) and pyrophosphate. NO activates sGC by binding directly to the heme moiety to form a ferrous-nitrosyl-heme complex. NO binds to the sixth position of the heme ring, breaking the bond between the axial histidine and iron, and forms a bond with iron. This results in a 5-coordinated ring where NO is now in the fifth position. Removal of heme results in loss of NO responsiveness [37]

Stimulation of guanylyl cyclases and the resultant accumulation of cGMP regulates complex signaling cascades through downstream effectors, including cGMP-dependent protein kinases (PKG), cGMP-regulated phosphodiesterases (PDE), and cyclic nucleotide-gated ion channels (CNGC) and thereby plays a central role in the regulation of diverse physiological processes, including vascular smooth muscle motility, intestinal fluid and electrolyte homeostasis, and retinal phototransduction [37].

PKG is the major receptor protein for cGMP in smooth muscle and the more abundant Iα -isoform of this enzyme mediates the ability of cGMP to relax contracted vascular smooth muscle. PKG is maintained in an inactive state by an auto-inhibitory domain. cGMP binds to a critical threonine residue causing conformational changes in PKG. This disrupts interactions between catalytic and auto-inhibitory domains and activates the enzyme. The cGMP-PKG pathway decreases the sensitivity of the contractile apparatus for calcium by altering myosin

light chain kinase activity which is important in the control of smooth muscle reactivity, platelet reactivity and cardiac function [38].

NO also forms complexes with non-heme metal containing proteins including iron-sulfur (Fe-S) as well as zinc-containing proteins. For example, ·NO disrupts the [4Fe-4S] cluster in aconitase, inactivating the enzyme. Thus NO has an inhibitory effect on oxidative phosphorylation by blocking the electron transport chain and controlling the levels of citrate in the Krebs cycle.

Zinc sulfur clusters also represent molecular targets for NO and its reactive nitrogen oxide intermediates. Kroncke, Kolb-Bachofen and colleagues have shown that NO can nitrosylate various zinc dependent transcription factors [39] and modify their contribution to gene expression [40]. For example, they originally noted that NO caused the release of zinc from Sp1 and EGR-1 [41] resulting in loss of their DNA binding activity. NO also interfered with the dimerization of vitamin D3 receptor and retinoid X receptor [42] affecting their transcriptional activity. In intact cells, NO was shown to inhibit IL-2 expression secondary to its S-nitrosylation of zinc dependent transcription factors [41]. These authors suggest that NO disruption of zinc fingers is an important aspect of the ability of NO to modify gene expression and outline a schema in which activation and/or inhibition may account for specificity of this novel pathway [42, 43].

2.1.4 Indirect effects of NO [36]

2.1.4.1 Reaction with superoxide ($O_2^{\cdot -}$)

The cGMP-independent effects of NO and its related oxidation products are not yet well described but have recently become a subject of intensive effort. The chemistry involved includes reactions between NO and other free radicals like superoxide ($O_2^{\cdot -}$) to produce the toxic species, peroxynitrite ($ONOO^-$) (Equation 2).

$$\cdot NO + O_2^{\cdot -} \rightarrow ONOO^- \quad (2)$$

Peroxynitrite is a potent cytotoxic molecule that can oxidize thiols [44] and DNA bases [45] and initiate metal independent lipid peroxidation [46]. At physiological conditions, the conjugate acid of peroxynitrite, ONOOH, has the ability to have hydroxyl radical reactivity. In the presence of iron, peroxynitrite can undergo heterolytic cleavage to form nitronium-like compounds (NO^{2+}) that can nitrate phenolic compounds including the aromatic rings of tyrosine.

2.1.4.2 Nitrosation of cysteine thiols

NO also reacts with molecular oxygen (O_2) to form nitrogen dioxide (NO_2) (Equation 3). The kinetics of this reaction is second order with respect to ·NO [36], and therefore this process (Equation 3) is relatively slow in aqueous solution under physiological conditions, where NO concentrations are low (<1 μM).

$$2 \cdot NO + O_2 \rightarrow 2NO_2 \quad (3)$$

However, NO and O_2 are >20 times more soluble in the lipid fraction of a cell and so the rate constants in lipid phase are greater than the aqueous phase. Thus the disposition of NO in

water is dominated by the formation of dinitrogen trioxide (N_2O_3) and nitrous anhydride (HNO_2) (Equation 4 and 5).

$$2\ NO_2 + \cdot NO \rightarrow N_2O_3 = +ON\ldots NO_2^- \quad (4)$$

$$N_2O_3 + H_2O \rightarrow 2\ HNO_2 = 2NO_2^- + 2H^+ \quad (5)$$

These species formed near lipophilic membrane are important because they account for the major disposition of NO in oxygenated water, nitrite (NO_2^-) that forms the basis of transnitrosation [47]. Probably the most commonly studied sGC-independent NO signaling pathway involves the S-nitrosation of low molecular weight thiols or protein thiols to form nitrosothiols which have been suggested to act as storage molecules or carriers of NO [48]. Equation (6) shows nitrosation of thiols result in S-nitrosothiols (SNO).

$$N_2O_3 + RSH \rightarrow RSNO + HNO_2 \quad (6)$$

In this reaction, R-SH can be either a protein thiol group or a small organic thiol, such as glutathione. Small organic thiol groups are present in millimolar concentrations in cells [49] and once they have been S-nitrosated they can serve as NO donors themselves (Equation 7, See also section: 2.1.3).

$$2\ RSNO \rightarrow RSSR + 2NO \quad (7)$$

Thus protein thiol groups can be either primary or secondary targets for NO-related species.

2.1.5 Regulation of RSNOs

Nitrosothiols have the ability to act as NO^+, ·NO, and NO^- donors [36] via either homolytic or heterolytic cleavage of the S-NO bond to produce ·NO , or NO^+ or NO^-, respectively [50].

Homolytic decomposition:

$$RS — NO \rightarrow RS\cdot + \cdot NO \quad (8)$$

Heterolytic decomposition:

$$RS — NO \rightarrow RS^+ + NO^- \quad (9a)$$

$$RS — NO \rightarrow RS^- + NO^+ \quad (9b)$$

A number of SNO compounds have been identified *in vivo*, including S-nitroso derivatives of the major endogenous thiols, such as S-nitrosocysteine, S-nitrosoglutathione, and S-nitrosoalbumin. Numerous proteins have now been identified as targets for nitrosation with resultant effects on protein function [51]. S-nitrosation of both the cardiac ryanodine receptor [52] and the N-methyl-D-aspartate (NMDA) receptor [53] have been associated with altered channel activity. In addition, the S- nitrosation of critical cysteine(s) in the active site of a number of enzymes, including those in the caspase family [54] has been associated with changes in activity.

Physiological studies have demonstrated that SNO bioactivities may also be stereoselective in that bolus injection of derivatives of the L -isomer of S-nitrosocysteine into the NTS of rats were associated with changes in cardiovascular and respiratory parameters, whereas the D -isomer of S-nitrosocysteine was inactive [55, 56].

2.1.6 S-Nitrosation of metallothionein (MT)

Proteins with zinc-thiolate clusters, such as metallothionein (MT) are also targets for nitric oxide [57, 58]. Metallothionein is a 6- to 7-kDa intracellular cysteine rich (30 mol%) heavy metal (Zn, Cd, Cu) binding protein. MT is critical to intracellular Zn^{2+} homeostasis with the ability to bind up to seven zinc atoms per mol MT [58, 59]. The *in vitro* data shows that NO causes protein unfolding and release of zinc [39], copper [60] or cadmium [61] from the thiolate clusters. More recently, live cell microscopy was used to show the interaction between green fluorescent protein (GFP)-modified target MT and NO in mammal endothelial cells (FRET-MT reporter molecule). The *in vitro* studies with this chimera protein (FRET-MT) in combination with NO donors, demonstrate that fluorescence resonance energy transfer (FRET) can be used to follow conformational changes indicative of metal release from MT (see section: 2.2.5).

2.1.7 Methods of NO detection

Direct measurement of NO is difficult, both because of the small amounts present (usually less than nM concentrations) and the labiality of NO in the presence of oxygen. NO is currently measured by spectroscopic methods, including chemiluminescence [62, 63], ultraviolet (UV) visible spectroscopic [64], and electron paramagnetic resonance (EPR) [3].

Chemiluminescence detection is being used as a tool to identify and quantify the cellular targets and the oxidative metabolites of NO, rather than directly measuring NO production. These forms include heme-NOs, S-nitrosothiol (RSNOs), N-nitrosamine (RNNOs), and nitrite. The assay is based on the measurement of the intensity of the fluorescent radiation emitted after chemical oxidation of NO by ozone using a sensitive photomultiplier tube (PMT). The product

of this reaction (NO_2^-) emits a photon, and the total number of photons produced is proportional to the NO concentration [65]. The UV visible spectroscopic method for NO determination is based on the Griess reagent which is a mixture of sulfamilamide, HCL, and N-(1-napthyl)-ethylenediamine (NED). The spectrum of the product of this reaction shows a band at 548 nm (Molecular Probes). The absorbance of this peak is proportional to the NO concentration.

A second UV visible spectroscopic method is based on the reaction of oxyhemoglobin (HbO_2) with NO to form methemoglobin (metHb) and nitrate (NO_3^-) and is used to determine rates of NO production. The reaction is also accompanied by significant changes in the absorption spectrum of HbO_2. The spectral changes form the basis of the hemoglobin NO assay, a well-established spectrophotometric technique that allows the quantification of NO in solution [66].

Electron paramagnetic resonance (EPR) can be used to monitor molecules with unpaired electrons including radicals such as ·NO. Since unpaired electrons are too low in concentration and short-lived to be directly detected by EPR in biological systems, this dilemma can be helped by EPR measurement of more stable secondary radical species formed by adding exogenous spin-trap-molecules such as hemoglobin to stabilize ·NO. Spin traps are compounds that interact with unstable radicals, producing a more stable adduct such as nitrosyl-hemoglobin (NO-Hb) that can be detected by EPR.

The methods described vary significantly in their invasiveness and sensitivity. The best method is the one that provides the best compromise for a given experiment. In general, the gas phase methods (chemiluminescence, spectrophotometric) are very sensitive, but tissues have to be extracted and/or chemically treated to release their NO. Also, there is still much controversy concerning the protocols that release NO from the sample. For instance, the values reported

from chemiluminescence method for concentrations of RSNO in plasma range from low-nanomolar to a few micromolar [67].

2.1.8 Alternative approaches - live cell fluorescent microscopy

Detection of interactions between target proteins and nitric oxide species typically requires disruptive biochemical techniques that preclude or limit temporal-spatial information. While the methods described in the previous section are useful in providing static information about the cellular state, live cell microscopy can be used to monitor the effects of individual molecules, and the interactions between molecules over extended periods of time, and in 3-dimensional space.

The 4,5-diaminofluoresceins (DAF-2) [68, 69] are among the most common fluorescent dyes that have been used to detect reactive oxygen (ROS) and nitrogen (RNS) species. Early *in vitro* studies demonstrated that these reporters are highly sensitive to physiological concentrations of NO (2-5 nM). These complexes have been rendered cell permeable with the addition of acetate groups (DAF-2 DA), which are removed by intracellular esterases, effectively trapping the reporter inside the cell. DAF-2 DA has been widely used [5] to detect and image ·NO but is hampered by concerns regarding its selectivity [6, 7], sensitivity [6], and interactions with divalent cations [8] in biological samples.

The recent development of genetically encoded fluorescent reporters based on green fluorescent protein have recently proven useful in detecting NO signaling pathways, as well as post-translational protein modifications induced by NO-related species, in living cells [10, 13]. These methodologies will be described in more detail in subsequent sections.

2.2 LIVE CELL FLUORESCENT MICROSCOPY

2.2.1 Principles of fluorescence

The principle of fluorescence microscopy depends on the inherent property of material that can be made to fluoresce (fluorophore) to emit a photon of a known energy (or wavelength) after appropriate excitation. Fluorescence activity is sometimes depicted as shown in a simplified theoretical excitation - Jablonski energy diagram (Figure 1).

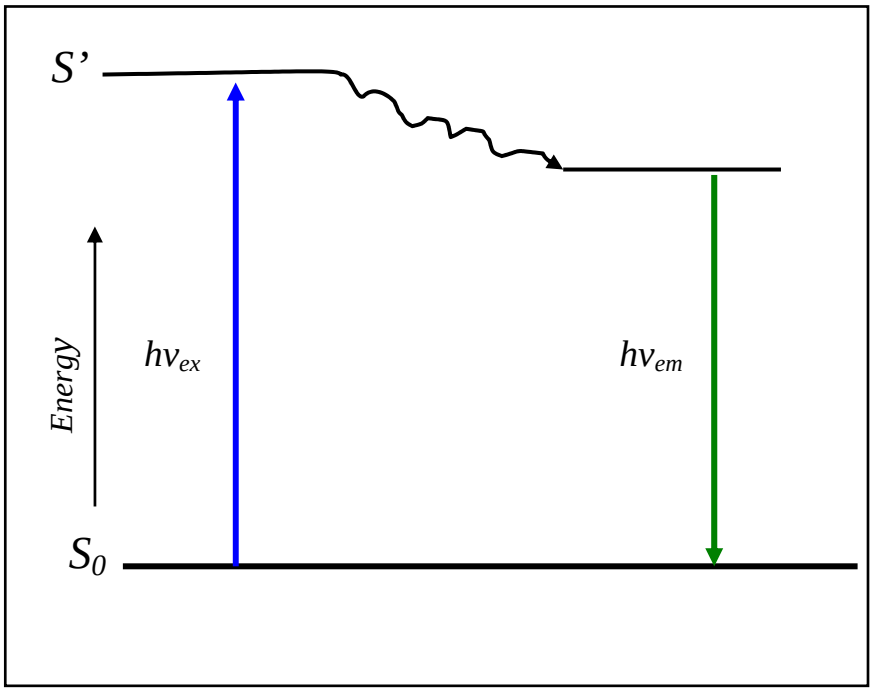

Figure 1 Simplified Jablonski energy diagram.

Prior to excitation, the electronic configuration of the molecule is described as being in the ground state. Upon absorbing a photon of excitation light electrons are raised to a higher energy and vibrational excited state. The excited electrons may lose some vibrational energy to the surrounding environment and return to what is called the lowest excited singlet state. From the lowest excited singlet state, the electrons are then able to "relax" back to the ground state with simultaneous emission of fluorescent light.

Different electrons have different rotational and vibrational energies. Moving to singlet state demands change to an equivalent vibrational or rotational energy at a higher electrical state. If the ground state changes, then the energy (of the photon) to get to a singlet state may also change. The energy required depends on the electrical, rotational, and vibrational energy needed to move electrons between specific states.

The wavelength difference between the excitation and emission light is known as the Stokes shift (Figure 2) and is the essential principle behind all fluorescence measurements. The greater the Stokes shift, the easier it is to separate excitation light from emission light. The emission intensity peak is usually lower than the excitation peak; and the emission curve is often a mirror image of the excitation curve, but shifted to longer wavelengths. To achieve maximum fluorescence intensity, the fluorochrome is usually excited at the wavelength at the peak of the excitation curve, and the emission is selected at the peak wavelength (or other wavelengths chosen by the observer) of the emission curve. The selections of excitation wavelengths and emission wavelengths are controlled by appropriate filters. In determining the spectral response of an optical system, technical corrections are required to take into account such factors as glass transmission and detector sensitivity variables for different wavelengths (http://microscope.fsu.edu/primer/lightandcolor/fluorescencehome.html).

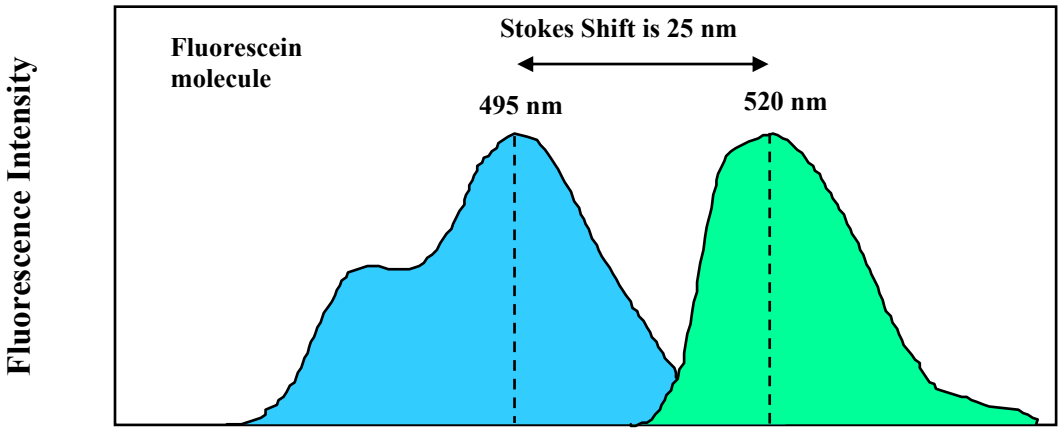

Figure 2 Stoke's shift diagram for fluorescein.

2.2.2 General principles of laser scanning confocal microscopy (LSCM)

The confocal microscope enables the optical sectioning of a 3D specimen without the need to employ some of the invasive methods used traditional histology. Information can be collected from a single focal plane of a fluorescently labeled biological specimen. The laser beam excites a point on the specimen. The emitted, longer-wavelength fluorescent light collected by the objective lens passes through the dichroic mirror (beam splitter) and any necessary emission filters and then is focused onto a light sensitive-detector (photomultiplier tube, PMT). A confocal pinhole excludes out-of focus light from above and below the focal plane resulting in an increase in image resolution. The laser beam then moves to the next point and another pixel is collected. The light detected by the PMT is associated to a pixel (picture element) on the monitor. By moving the focal plane of the instrument step by step through the

depth of the specimen a series of optical sections can be recorded. The sections collected can subsequently be reconstructed in three dimensions. (http://www.zeiss.com)

2.2.3 Live cell imaging

Traditional biochemical and/or molecular biology approaches provide static information about the cellular state whereas live cell microscopy can be used to monitor the effects of individual molecules, and interactions between molecules, on cell development, organization and fate over extended periods of time, and in three-dimensional space.

The imaging of living cells has necessitated the development of new methodologies to allow multi-parametric analysis while maintaining functional viability over extended time periods. Most laboratories utilize completely automated imaging systems equipped with temperature controlled stage inserts to maintain 37°C. Maintaining the cells at physiological pH can be achieved by imaging cells in media containing bicarbonate or phosphate buffers such as HEPES buffered saline or Hanks balance salt solution (HBSS) without phenol red (which causes background fluorescence).

Individual live cell imaging systems must be designed very carefully for the intended application, cell type and environment. The duration and intensity of illumination must be minimized to maintain cell viability and therefore the sensitivity of the detector is of critical importance. Automated shutters, and filter wheels or monochromators which enable rapid switching of excitation wavelengths, are essential to minimizing light exposure and enhancing the speed of data acquisition. In addition, the choice of objectives is critical for all live cell work. The most useful optics are the 20X 40X and 60X. A 20X is used for surveying cell

populations whereas a 60X is essential for subcellular imaging. These objectives should have the highest numerical aperture (NA) available for the type of transition media used.

2.2.4 Fluorescent labeling of cells and molecules for live imaging

Two main categories of fluorophores (fluorochromes) are: 1) dyes or reagents; and 2) genetically encoded fluorescent proteins.

2.2.4.1 Fluorescent dyes

Traditional dyes include ion-specific and/or pH sensitive probes (SNARF), reporters for reactive oxygen and nitrogen species (DAF), synthetic organic compounds (PBFI for K^+ detection, Fura-2 for Ca^{2+} and Fluozin-3 for zinc). Dyes are available that report specific cellular compartments, such as mitochondria, Golgi apparatus, or lysosomes. Finally, fluorophores have been incorporated into many enzyme substrates to allow monitoring of enzyme activity. Many of the fluorescent probes suitable for use in biomedical research were developed by, and are commercially available from Molecular Probes (www.probes.com).

It is important to recognize that the sensitivity or specificity of fluorescent indicators may be reduced by a variety of factors. Problems due to photobleaching, autofluorescence, scattering, and absorption are encountered commonly. In addition, cross talk between fluorophores can be problematic with the use of multiple probes.

2.2.4.2 Protein-based indicators - green fluorescent protein (GFP)

Green fluorescent protein (GFP) is a spontaneously fluorescent protein originally isolated from the Pacific jellyfish, *aequorea victoria*. The fluorophore in GFP is derived from three

consecutive amino acids (aa) from: Ser-65, Tyr-66, and Gly-67 (at positions 65-67 in the protein). After synthesis of GFP, these three aa undergo autocatalytic cyclization and oxidation to form the functional fluorophore. The fluorophore contains a series of conjugated double bonds that result in the fluorescent properties of GFP [70].

GFP has several qualities that make it ideal for *in vivo* imaging. First, GFP can be expressed in a variety of cells, where it becomes spontaneously fluorescent without the need for cofactors. Second, because it is a protein (GFP consists of only 238 aa), GFP can be tagged with an appropriate signaling peptide and expressed as such or fused to another protein at either the COOH or NH_2 termini in specific organelles, such as the mitochondria, the nucleus, or the endoplasmic reticulum without affecting native function or localization. Third, GFP is highly stable. Therefore, in addition to being imaged in living cells, it can also be used in fixed or frozen cells and tissue. GFP has been successfully used for many years as a marker for studying gene expression as well as protein folding, trafficking, and localization and for monitoring complex processes, such as intracellular second messenger dynamics, enzyme activation, and protein-protein interactions [7, 9].

Mutations within the three aa fluorophore have produced a variety of GFP variants with differing spectral characteristics, thus increasing the number of potential uses for GFP. For example, a double mutation of Phe-64 to Leu and Ser-65 to Thr yields enhanced GFP (EGFP), the most commonly used GFP variant. This variant exhibits a red-shifted excitation maximum from 395 nm (wild type) to 488 nm, allowing for the use of standard FITC optics, and it is more photostable and sixfold brighter than wild-type GFP. The development of GFP variants with differing absorbance and emission spectra has allowed for the simultaneous visualization of multiple tagged molecules within a cell. In particular, the pairing of the cyan (CFP) and yellow

(YFP) fluorescent proteins has been instrumental in advancing the use of fluorescence resonance energy transfer (FRET) to investigate inter- and intramolecular interactions in living cells [71].

2.2.5 Florescence resonance energy transfer (FRET)

Fluorescence resonance energy transfer (FRET) is a nondestructive spectrofluorometric technique. In combination with scanning laser confocal microscopy, FRET is capable of detecting changes in the conformational state of proteins in live cells.

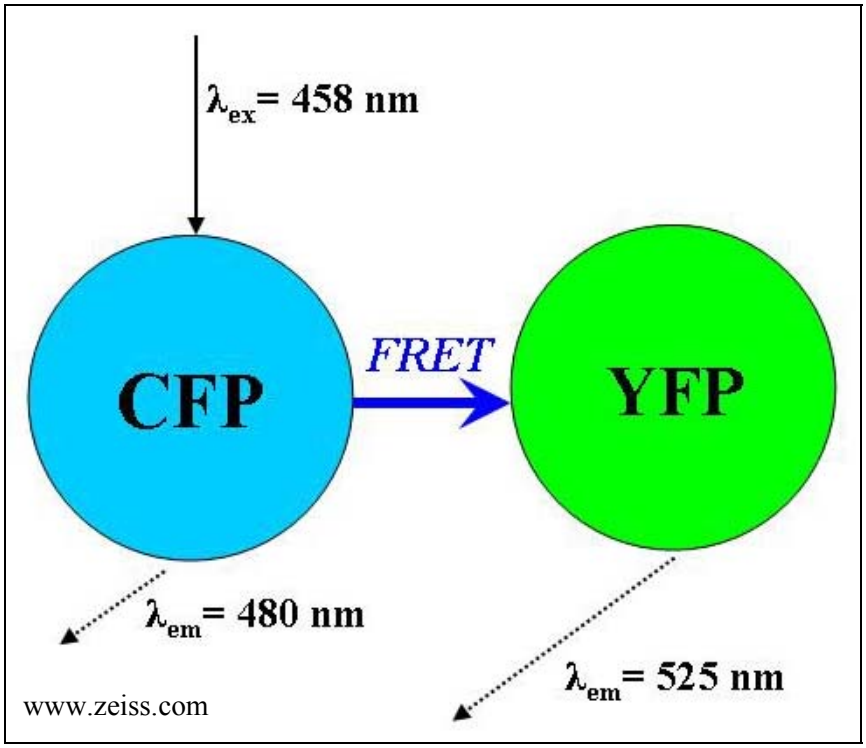

Figure 3 Basic principles of Florescence resonance energy transfer (FRET). The donor fluorophore is excited. When the donor is in close proximity (1-10 nm) to the acceptor fluorophore (YFP) excited state energy will be transferred non-radiatively to the acceptor resulting in a quenching of the donor emissions and the emission of light from the acceptor. (www.zeiss.com).

The basic principle of FRET (Figure 3) is the transfer of energy from an excited donor fluorophore to an appropriately positioned acceptor fluorophore without associated radiation release (no photons are emitted from the donor). FRET can occur when the emission spectrum of the donor overlaps (> 30%) with the absorption spectrum of the acceptor.

The energy transfer efficiency (*E*), are calculated using the Förster's formula:

$$E = \frac{1}{[1 + (R / R_0)^6]} \quad ;$$

R is the distance between the donor and acceptor molecule and R_0 is the distance at which 50% of the energy is transferred. As the efficiency of energy transfer is related to the inverse of the sixth power of the distance separating the donor and acceptor fluorophores, the distance over which FRET can occur is limited to between 1 and 10 nm. Also for example, the doubling of the distance between the 2 fluorophores, for example from R_0 to $2R_0$, will decrease the efficiency of transfer from *E*=50% to *E*=1.5%. Therefore, FRET provides a very sensitive measure of intermolecular distances and of conformational changes in GFP-modified proteins [72].

Because of its strong distance dependence, FRET has been used to evaluate the proximity and interaction of molecules and to visualize their dynamic behaviors in intact living cells. Other factors such as the overlap of the emission of the donor with the absorption of the acceptor and the relative orientations of the two fluorophores also affect the energy transfer.

2.2.6 FRET detection using spectral imaging

Conventional methods for detecting FRET between a donor and an acceptor with overlapping excitation and emission spectra require the use of narrow detection bands and

automatic switching of optical filters to differentiate between emissions, along with complex mathematical corrections to account for crosstalk between channels. Recent advances in detector technology, however, now enable the resolution of fluorescent images providing full spectral information (Figure 4) for each voxel of the image without switching of optical filters.

Furthermore, it is possible to unambiguously separate the cross-talk between overlapping cyan and yellow emissions using spectral imaging. The use of this method allows the detection of small, but potentially biologically meaningful, changes in FRET that are common with genetically encoded reporters and are extremely difficult to resolve reliably using more traditional methods relying on bandpass filters. Eliminating the use of bandpass filter-based detection systems also removes the limitations on the number of fluorophores that can be detected reliably in a single sample. Spectral imaging systems use the spectral information and calibration spectra to calculate the actual amount of fluorescence originating from a particular fluorochrome, and therefore it is possible to measure multiple parameters synchronously based on the characteristic spectral profile of a given fluorophore. This procedure is referred to as "unmixing" the emission spectrum (www.zeiss.com).

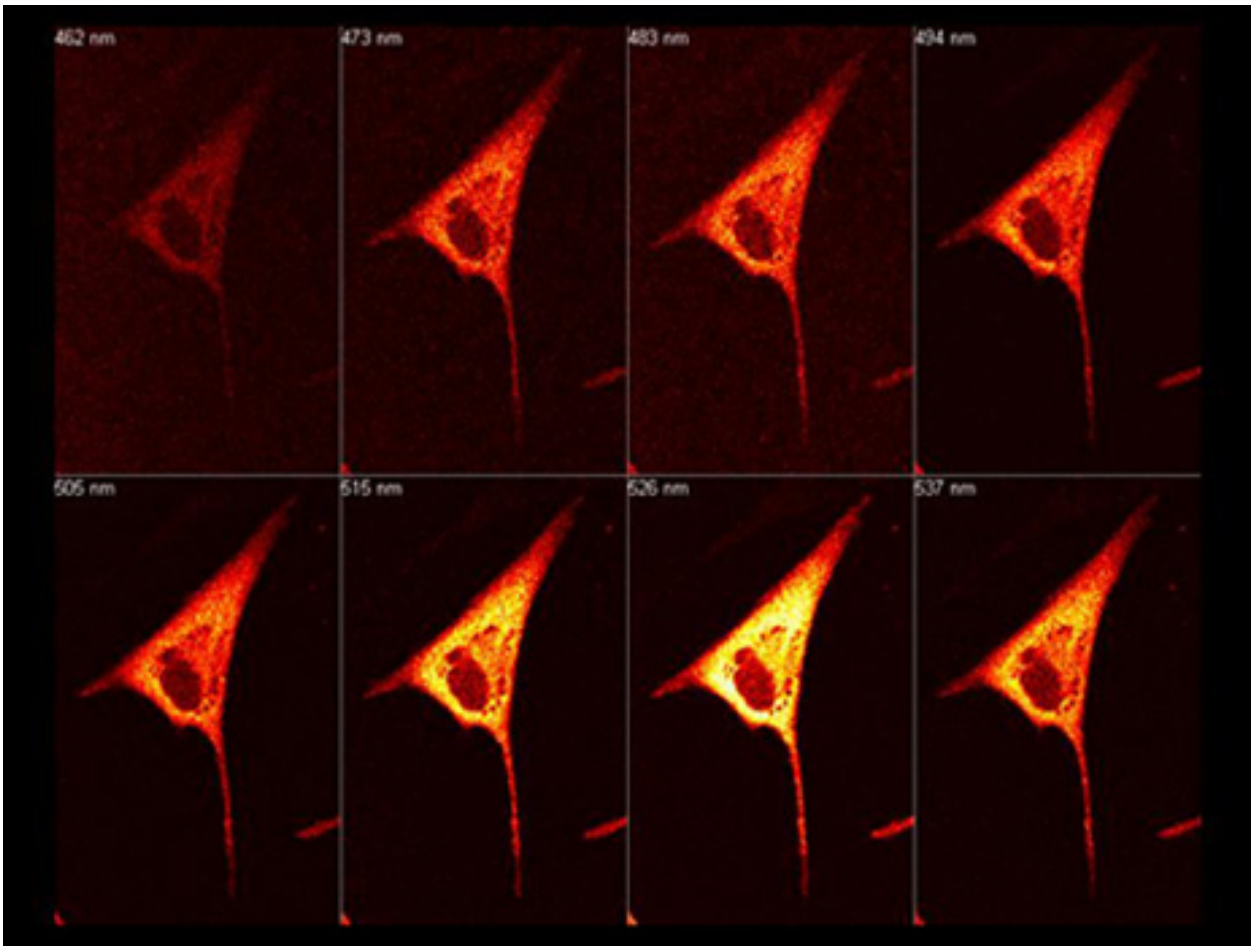

Figure 4 Spectral imaging of FRET-MT in live sheep pulmonary artery endothelial cells. Lambda acquisition of a single cell imaged using the Zeiss LSM510 META (see Methods). The sample was excited with the 458 nm line of Argon laser and the fluorescence signal was split into eight channels for detection of emissions at ~10 nm increments ranging from 462-537 nm.

2.2.7 FRET measurement

Two common ways to quantify FRET using live cells microscopy are: 1) ratioing of emission measurements, and 2) acceptor photobleaching.

2.2.7.1 FRET ratio

The basic principle of FRET involves the transfer of a fraction of the excited state energy from the donor CFP molecule to the acceptor resulting in fluorescence emissions detected at 525 nm (acceptor, YFP). The intensity of the emitted signal will depend on the efficiency of transfer. The FRET interaction will also diminish or quench the emissions from the donor fluorophore, CFP (480 nm). Without a FRET partner, an excited donor molecule returns to its ground state, emitting photons with wavelengths which peak around 480 nm for CFP.

The FRET ratio is the ratio of the emission intensity of the acceptor fluorophore divided by the emission from the donor fluorophore while the sample is excited at the excitation wavelengths specific to the donor fluorophore. The calculated ratio is proportional to the degree of physical association between the two fluorophores. For the CFP and YFP pair, the FRET ratio is obtained by dividing the emitted fluorescence intensity at 525 nm (YFP) by the emitted fluorescence at 480 nm (CFP) while the sample is excited at 430-458 nm.

While some degree of overlap in the spectra for the donor and acceptor fluorophores is required for efficient energy transfer, this also complicates the FRET measurements firstly because the CFP emission tails into the YFP channel; and secondly YFP is excited directly, although inefficiently, at the excitation wavelengths used for CFP. The use of calibration spectra combined with spectral unmixing is therefore useful in separating the emissions due to cyan and yellow individually without the need for complex mathematical manipulations.

2.2.7.2 Acceptor photobleaching

Acceptor photobleaching is commonly used as a control to confirm the presence of FRET [73]. This technique is based on the principle that the constant or repetitive illumination of the acceptor (in this case EYFP) leads to the irreversible photochemical destruction of the fluorophore. Accordingly, if FRET was occurring, the donor will become unquenched following bleaching of the acceptor reflected by an increase in donor emission. Such an increase in fluorescence following bleaching is particularly a valid confirmation FRET, because in most circumstances fluorescence normally decreases following photobleaching. Furthermore, increases in donor fluorescence cannot be related to acceptor bleed-through, because the acceptor has been made non-fluorescent.

2.2.8 FRET-based reporters

Two general strategies have evolved using GFP variants in FRET-based applications. The first strategy involves the encoding of GFP donor and acceptor fluorophores on distinct proteins to study intermolecular interactions. In this case, FRET between the two fluorophores provides direct evidence for a physical interaction between the two proteins and has now been widely used in living cells to support the *in vitro* data provided by immunoprecipitation, receptor-ligand binding, enzyme-substrate association/dissociation, or protein-nucleic acid interactions.

The second strategy involves the use FRET to study intramolecular events by incorporating the donor and acceptor fluorophores at two different ends of the same protein. Alterations in protein conformation change the relative positions of the two fluorophores and this

is reflected in alterations in FRET. This approach can be applied to the study of fluctuations and stability within a single macromolecule, or the dynamics of protein folding or unfolding.

The following series of experiments utilized physiology-based intramolecular FRET reporters that are targets for the following NO-related modifications: a) S-nitrosation, via the cysteine-rich protein, metallothionein (FRET-MT); and b) nitrosyl-heme-Fe, via guanosine 3′,5′-cyclic monophosphate (cygnet-2) to detect signaling events in pulmonary endothelium.

2.2.8.1 FRET-MT reporter

In order to study the interaction between the heavy metal-binding protein, metallothionein (MT) and NO in live cells, Pearce et al. designed a chimeric construct (called FRET-MT) based on calmodulin reporter, cameleon [9]. Figure 5 shows the FRET-MT cDNA construct of human type IIa metallothionein (hMTIIAa), flanked by enhanced cyan fluorescent protein (ECFP) and enhanced yellow fluorescent protein (EYFP). The combination of the 6-kDa MT with two 27-kDa GFPs resulted in the formation of a 60-kDa fusion protein (FRET-MT) as determined by SDS/PAGE analysis and Western blotting of transfected Chinese hamster ovary cell lysates [13].

The human MT protein binds seven zinc atoms and contains 60–68 amino acids, of which 20 are highly conserved cysteines. In one domain, three zinc atoms are bound to nine cysteines, whereas in the other domain, four zinc atoms are bound to 11 cysteines [59]. The donor (ECFP) and the acceptor (EYFP) in double-labeled MT are at a distance suitable for energy transfer (FRET) which allows monitoring of events such as metal binding and conformational changes in the protein domain [71]. *In vitro* studies with this chimera (FRET-MT) has shown that FRET can be used to follow conformational changes indicate the metal release from MT [13].

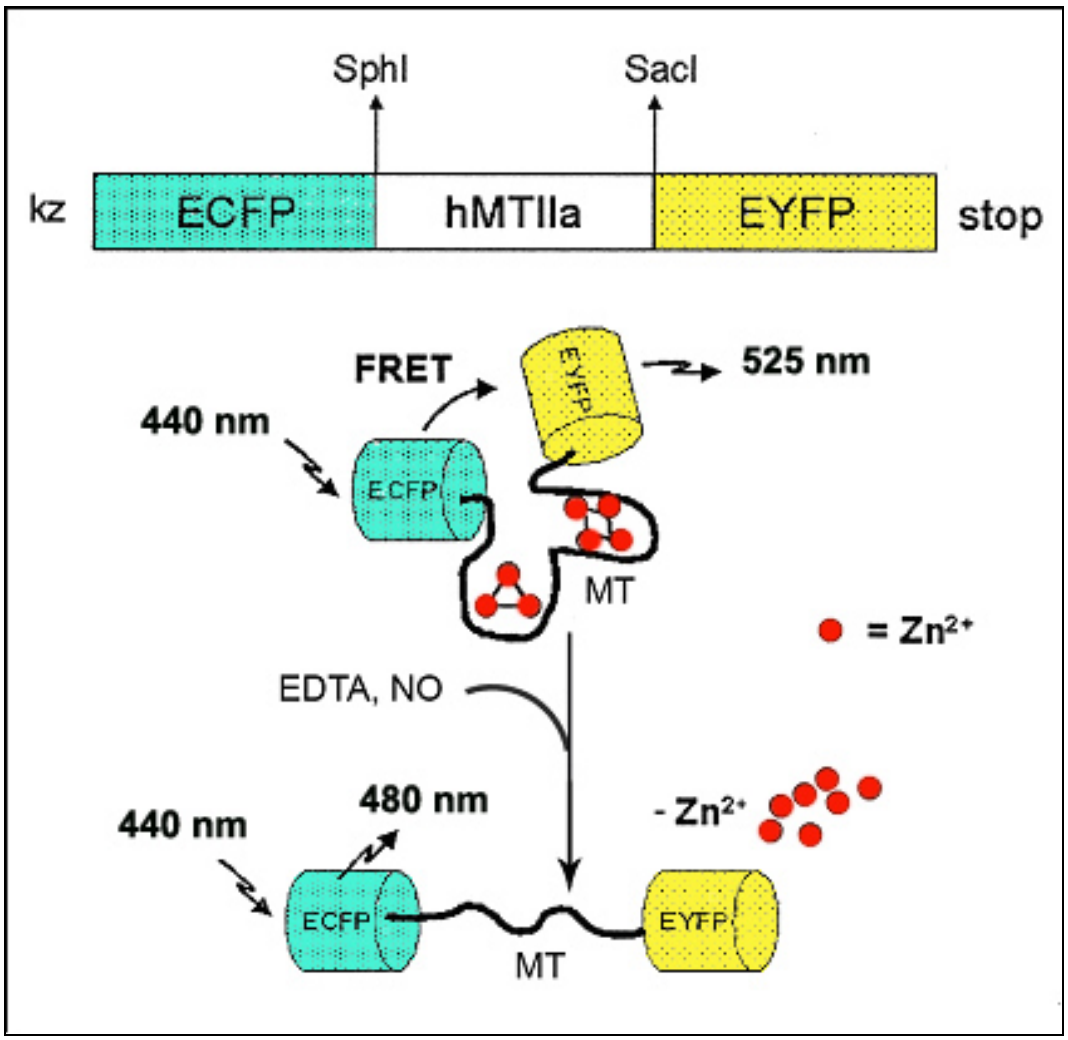

Figure 5 FRET-MT reporter construct. Scheme of the FRET-MT reporter construct of human type IIa metallothionein, flanked by enhanced cyan fluorescent protein (ECFP) and enhanced yellow fluorescent protein (EYFP) showing unfolding, metal release and consequent changes in FRET induced by metal chelators or nitric oxide (NO) [13].

2.2.8.2 Cygnet-2 reporter (cGMP indicator using energy transfer) [10]

The cygnet-2 reporter is based on a truncated form of protein kinase G Iα (PKG Iα) and was designed to visualize the dynamics of the guanylate cyclase/ cGMP pathway in living cells. The conformationally active cGMP-binding domain was sandwiched between enhanced versions of cyan and yellow fluorescent protein to modulate FRET between the two chromophores (Figure 6). PKG Iα with an N-terminal deletion was chosen because it is the most ubiquitous physiological sensor of cGMP and is conformationally sensitive to cGMP. Furthermore, it is closely related to cAMP-dependent protein kinase, from which indicators had already been engineered [11, 12]. Direct binding of cGMP to the PKG domain of cygnet-2 induces a conformational change that can be recorded as a decrease in intramolecular FRET between ECFP and EYFP. The kinase activity was eliminated by mutating, Thr^{516} of cGMP-dependent protein kinase (cGPK) to Ala.

To test the FRET response of cygnet to cGMP, the soluble guanylate cyclases were activated by the application of the NO donor, SNAP. This led to a rapid ratio increase, reaching a steady state within a minute. After drug washout, the FRET signal recovered to the basal level. This indicates that NO induces a very rapid and reversible increase of cGMP that can be monitored in real time in living cells [10].

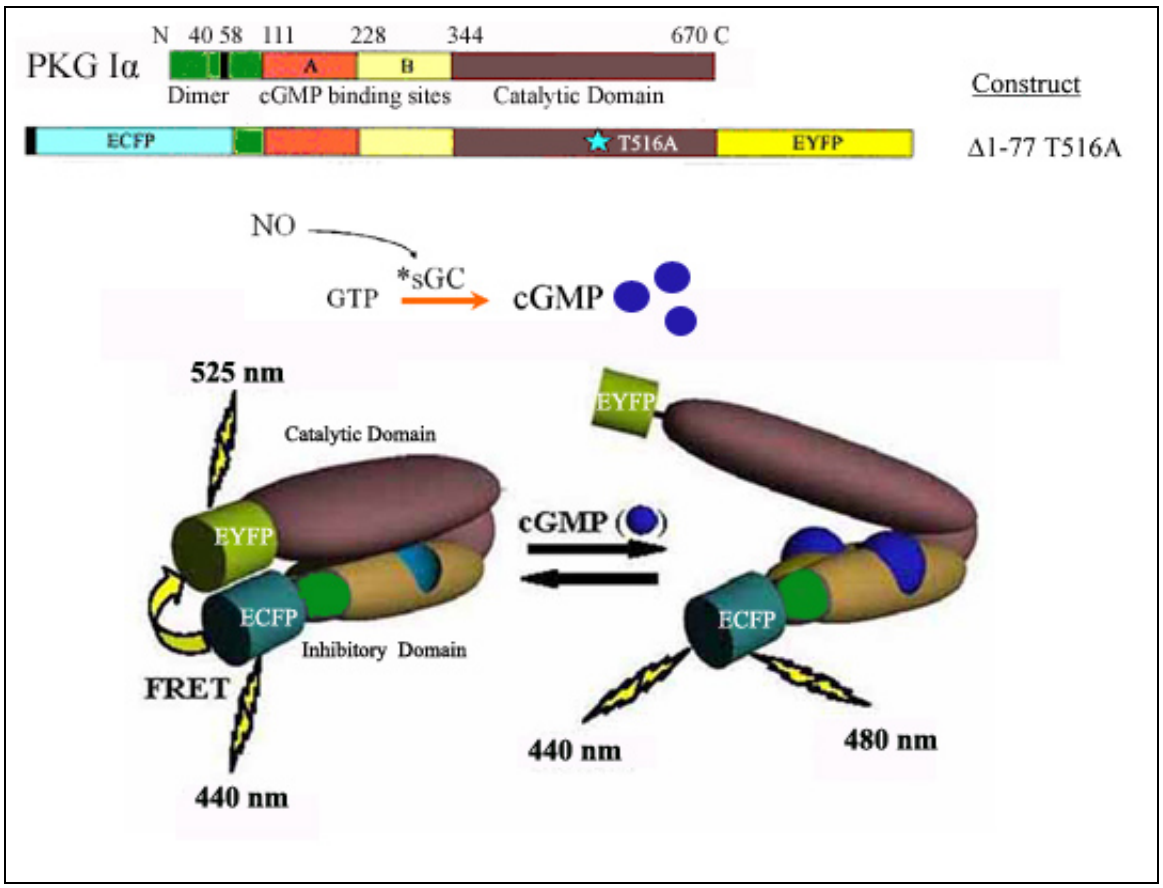

Figure 6 Cyclic guanosine monophosphate (cGMP) reporter, cygnet-2 construct. Domain structure of FRET-based cGMP-indicator: N-terminal cGPK deletion mutants: Δ1-77/Thr516Ala (cygnet-2) represents the catalytic inactive mutant [10]. A sensitive cGMP-binding fragment of PKG is sandwiched between cyan fluorescent protein (ECFP) and enhanced yellow fluorescent protein (EYFP). (Image is modified from **http://www.uvm.edu/~wdostman/Dostmann_Lab.htm**)

3.0 EXPERIMENTAL METHODS

3.1 EXPERIMENTAL DESIGN

NO is a diffusible, multifaceted transcellular messenger that exerts its influence on a myriad of biological functions in a cGMP-dependent fashion. Nonetheless it is apparent that post-translational modifications of protein, in a cGMP-independent fashion, may significantly contribute to the diverse actions of NO. NO-related species, including ·NO, NO^+ and NO^- have been shown to be important both pharmacologically and physiologically. The overall objective was to use FRET-based technologies to distinguish between signaling events that are mediated by the free radical ·NO, as is best exemplified by the activation of soluble guanylyl cyclase (sGC), and direct transnitrosation of cysteine thiols via NO^+. We used a confocal-based spectral resolution approach to visualize the effects of membrane permeant forms (ethyl esters) of the D- and L- stereoisomers of S-nitrosocysteine on FRET-based reporters for cGMP (cygnet-2) and for the cysteine-rich, metal binding protein, metallothionein (FRET-MT).

3.2 SPECIFIC PROTOCOLS

3.2.1 Isolation and culture primary sheep pulmonary artery endothelial cells

Sheep pulmonary artery endothelial cells (SPAEC) were isolated from sheep pulmonary arteries obtained from a nearby slaughterhouse as previously described [74]. Cells were harvested by collagenase type I (0.1 %; Sigma, St. Louis, MO) digestion (37ºC; 30 min) and transferred to 35-mm plastic tissue culture dishes. Cells were expanded in Optimem (GIBCO, Grand Island, NY) with endothelial cell growth supplement (15 µg/ml; Collaborative Biomedical Products, Bedford, MA), heparin sulfate (10 U/ml), penicillin (100 U/ml), streptomycin (100 µg/ml) and 10% fetal bovine serum (Sigma, St. Louis, MO). Cells were grown in the above medium at 37ºC in 95% air-5% CO_2. They were routinely passaged 1:3 by detaching cells with a balanced salt solution containing trypsin (0.05%) and EDTA (0.02%). At the second to third passage, a T-75 flask (~3-5 x 10^6 cells) was incubated with 1,1′-dioctacedyl-1,3,3,3′,3′-tetramethyl-indocarbocyanine perchlorate-labeled acetylated low-density lipoprotein (Dil-Ac-LDL; Biomedical Technologies, Stoughton, MA) in growth medium for 4 h at 37ºC, washed, trypsinized, and resuspended in growth medium. Cells preferentially incorporating Dil-Ac-LDL were obtained by fluorescent-activated cell sorting (FAC-star, Becton Dickinson Immunocytometry System, San Jose, CA) [75]. Subsequently, subpassages were routinely homogeneously positive for Dil-Ac-LDL uptake as well as factor VIII-related antigen. SPAEC were used between passages 6 and 12.

3.2.2 FRET-MT reporter

The FRET-MT construct was designed by Pearce et al. [13] following the example of the calcium indicator cameleon-1 [9] in which a yellow green fluorescent protein (GFP) variant (EYFP) and a cyan GFP variant (ECFP) were fused to the COOH and NH2 termini, respectively, of human MT-IIA (FRET-MT) [13].

An E1-and E3 deleted replication-deficient adenoviral vector expressing hMT-IIA (AdV.MT) was constructed using a proprietary kit (Microbix Biosystems, Toronto, Canada) and a bacterial plasmid containing the MT insert [76]. Briefly, the MT cDNA, driven by a human cytomegalovirus promoter, was subcloned into a shuttle plasmid and cotransfected into 293 cells with a complimentary plasmid carrying the remainder of the circularized viral genome [77]). After recombination, plaque isolates were screened, and the selected clone was propagated in 293 cells, purified by three rounds of discontinuous CsCl step-gradient centrifugation, and desalted over a G-50 column. The titer for the AdV.MT preparation was 2.6×10^{11} plaque-forming units/ml. Infections were performed for 60 minutes with virus diluted in basal media to the desired multiplicity of infection of 50:1. Microspectrofluorometry was performed 24-48 hour after adenoviral infection.

3.2.3 Cygnet-2 (cGMP) reporter

The cDNA encoding a fluorescent cGMP indicator consisting of cGMP protein kinase G Iα (PKG Iα), minus residues 1–77, bracketed between cyan and yellow mutants of green fluorescent protein (cygnet-2) [10] was kindly provided by Roger Y. Tsien (University of California at San Diego). This reporter can detect changes in the activation of guanylyl cyclase

indirectly via structural changes in cGMP-dependent protein kinase [10]. SPAEC that expressed cygnet-2 were imaged 48 h after transfection with Lipofectamine Plus (GIBCO, Grand Island, NY).

3.2.4 Preparation of reagents

3.2.4.1 S-nitrosocysteine ethyl ester (SNCEE) synthesis

The hydrochloride of S-nitroso-L-cysteine ethyl ester was prepared via direct S-nitrosation of the hydrochloride of L-cysteine ethyl ester with ethyl nitrite, as previously described [78].

D-Cysteine ethyl ester was prepared as described by Baldwin [79]. Briefly, D-cysteine hydrochloride monohydrate was dissolved in dry distilled methanol, and HCl gas was bubbled through the solution for 2 hours and then stirred at room temperature (48 hours). The salient was rotor-evaporated at 20°C to yield oil which, upon titration with diethyl ether, yielded D-EtO-Cys-SH (99%) as white crystals. The product's purity was controlled by determination of free SH groups with 5,5′-dithiobis-2-nitrobenzoic acid [80] and by HPLC-EC [14].

3.2.4.2 OxyHemoglobin (HbO_2)

Human hemoglobin (Sigma, St. Louis, MO) was dissolved in Hanks' balanced salt solution (Gibco BRL) and reduced using a 10-fold excess of sodium ascorbate (Sigma, St. Louis, MO). Oxyhemoglobin (HbO_2) was purified by passing the solution over a Sephadex G-25 column and the concentration of HbO_2 was measured at an absorbance of 415 nm. Final concentrations of 100 μM HbO_2 were used in the described experiments.

3.2.5 Determination of nitrite concentration

Nitrite is one of the stable products formed from NO upon release from cells [32]. Two separate subcultures of SPAEC were exposed to 200 μM D- or L-SNCEE for 2 hours. The production of NO by treated cells was determined by measuring the accumulation of nitrite in the cell culture supernatant (Griess reaction). Aliquots of 100 μl of either standards or supernatants to be assayed were added to 96-well microtitre plates in triplicate followed by 100 μl of Griess reagent [0.1% N-(1-napthyl) ethylenediamine hydrochloride freshly mixed 1:1 (vol/vol) with 1% sulfanilimide in 5% phosphoric acid] [81]. The plates were left for 10 min at room temperature and then absorbance was measured using Fusion-α plate reader at 550 nm and nitrite was quantified with $NaNO_2$ as a standard.

3.2.6 FRET detection

Cells were bathed in Hanks' balanced salt solution without phenol red (Gibco BRL) containing 100 μM EDTA to chelate trace amounts of metal ions in the buffer and prevent extracellular decomposition of S-nitrosothiol, and imaged at 37°C using a thermocontrolled stage insert (Harvard Apparatus, Inc., Holliston, MA, USA).

Images were obtained with a 40× oil immersion optic at 512 × 512 pixels using the confocal-based Zeiss spectral imaging system (LSM510 META; Carl Zeiss, Jena, Germany). Cyan was excited at 458 nm (HFT 458). Resolved fluorescence spectra at each pixel were detected by an array of eight spectrally separate photomultiplier tube elements within the META detection head and recorded on a voxel-by-voxel basis during scanning to generate a set of images, each corresponding to the fluorescence wavelength resolved at 10 nm intervals. Color

separation of cyan and yellow emission spectra was determined from the resolved image using a linear unmixing algorithm based on reference spectra obtained in cells expressing only cyan or yellow protein. Images were collected at baseline and 1, 3, 6, and 9 min after addition of the relevant agonist and are stored as 12 bit TIFF images.

3.2.7 Control experiments

3.2.7.1 Acceptor photobleaching

In separate control experiments, selective acceptor photobleaching was performed to confirm the existence of FRET under baseline conditions. This technique is based on the principle that the constant or repetitive illumination of the acceptor (in this case EYFP) leads to the irreversible photochemical destruction of the fluorophore. Accordingly, if FRET was occurring, the donor will become unquenched following bleaching of the acceptor reflected by an increase in donor emission. A single cell within a field was chosen and EYFP was photobleached using the 514 nm line (at full power) of the argon laser. FRET transfer efficiency (*EFRET*) was calculated as a percentage using the formula:

$$EFRET = \frac{(I_1 - I_0)}{I_1} \times 100$$

where I_0 and I_1 represent ECFP intensity at baseline and following photobleach, respectively [73]. The same calculation was performed on non-bleached cells within the same field.

3.2.7.2 Timed bleach control

A second control was performed to determine the effects of repeated laser exposure on the FRET constructs and the calculated FRET ratios. In separate control experiments, a single field of cells was subjected to the 458 line of the argon laser exposure every 2 minutes with repeated scans over a 20 minute time frame to mimic the imaging conditions during experiments with D- and L-SNCEE.

3.3 DATA ANALYSIS

3.3.1 FRET data

The intensities for the emissions due to cyan and yellow were recorded for selected regions of interest (ROI) within individual cells under baseline conditions and following treatment with SNCEE. The FRET ratio (F_{525}/F_{485}) was calculated for each individual cell and mean data was obtained from three separate experiments under each condition, with 3-5 cells per experiments. Changes in FRET in response to D- and L-SNCEE were expressed as a percentage of baseline and reported as ± standard deviation.

3.3.2 Statistical analysis

Statistical comparisons of the percent change in FRET ratios between the L- and D-SNCEE treatment of FRET-MT or cygnet-2, were made using paired t-tests. Repeated-measures analysis of variance (ANOVA) with post-hoc Bonferroni tests [82] was used to compare the averages of pre and post treatment data from the three experiments. $P < 0.05$ was the criterion of significance. All data are represented as the mean SD (standard deviation).

4.0 RESULTS

4.1 CONTROLS

Selective acceptor photobleaching was performed as a control to confirm the existence of FRET under baseline conditions Figure 7 shows two endothelial cells expressing FRET-MT, following linear unmixing using calibration spectra for ECFP and EYFP. These images therefore represent the separate contributions of the cyan and yellow emissions (Figure 7a). The spectral report shows an increase in the peak emission intensity of the donor (ECFP, ~485nm) and a decrease in that of the acceptor (EYFP, ~525nm) in the single cell selected for photobleaching (Figure 7b). The estimates FRET efficiency were 24%, in the bleached cell, and 0.1% in the control cell.

A second control was performed to determine the effects of repeated laser exposure on the FRET constructs and the calculated FRET ratios. The field of cells shown in Figure 8 was exposed to repeated scans using the 458 line of the argon laser. The images of two endothelial cells expressing FRET-MT, shown in Figure 8 have undergone linear unmixing using calibration spectra for ECFP and EYFP and therefore represent the separate contributions of the cyan and yellow emissions (Figure 8a). The spectral report shows that exposing the cells to the 458 line of the argon laser every 2 minutes, over a 20 minute time frame had no effect in the peak emission intensity of either the donor (ECFP, ~485nm) or the acceptor (EYFP, ~525nm) (Figure 8b)

confirming that the observed changes in FRET following SNCEE are not likely due to selective bleaching of the YFP.

4.2 S-NITROSOCYSTEINE ETHYL ESTER (SNCEE) ACTIVATES FRET-MT REPORTER STEREOSELECTIVELY

SPAEC were infected with an adenovirus encoding the cDNA for a GFP chimeric protein, consisting of the 6 kDa heavy metal binding protein MT, sandwiched between enhanced cyan (ECFP) and yellow fluorescent protein (EYFP), as previously described [13, 14]. Traditional FRET detection methods using bandpass filters to separate cyan and yellow emissions have previously been used to show that this construct is sensitive to a variety of NO donors as well as agents that increase eNOS-derived NO [13, 14]. We have now extended these findings using the spectral imaging approach for FRET detection, in combination with a novel membrane permeant S-nitrosothiol, to provide further details regarding the biochemical nature of the nitrosative modifications of MT.

Figure 9a shows a single endothelial cell expressing the FRET-MT reporter after linear unmixing using calibration spectra for ECFP and EYFP. These images therefore represent the separate contributions of the cyan and yellow emissions. The spectral report for this cell appears in Figure 9c and shows an increase in the peak emission intensity of the donor (cyan, ~485 nm) and a decrease in that of the acceptor (yellow, ~525 nm) after application of L-SNCEE (50 μM).

In three subcultures of SPAEC expressing the FRET-MT reporter (3-5 cells per experiment) intra-molecular FRET was decreased on average by 30.2% ± 11.3% (SD) in response to L-SNCEE (Figure 9c and 10). These changes suggest nitrosothiol-induced

conformational changes in MT that are consistent with the previous reports of NO-mediated release of metals from thiolate clusters of the protein [14, 39]. In contrast to the effects of L-SNCEE on FRET-MT, there was no significant change in FRET in response to an equimolar concentration of D-SNCEE (Figure 9d and 10). However, both isomers of SNCEE activated protein kinase G Iα (PKG Iα) to a similar extent (see Figure 15 in the next section) suggesting that the stereoselective effect was specific to MT and most likely reflected a transnitrosation reaction.

In separate experiments L-SNCEE-induced changes in FRET were reversed by 50 μM dithiothreitol (DTT; Figure 11). Such reversibility is suggestive of nitrosothiol-mediated modification of a cysteine residue(s) in MT [83]. Furthermore, the effects of L-SNCEE on the FRET-MT reporter were not affected by HbO_2 (Figure 13 and 14), which would be expected to block any process involving ·NO liberated by decomposition of nitrosothiol, but would not necessarily affect transnitrosation [84, 85]. As expected, L-SNCEE decreased the FRET ratio by 23.6 ± 2.6 % (Figure 14).

D- and L-SNCEE decomposed equally in cell-based assays, as determined by the accumulation of nitrite in EDTA-free culture medium (data not included). In addition, both isoforms activated PKG Iα to similar extents, suggesting that the stereoselective effect was specific to MT. These combined results most likely reflected the transnitrosation of thiolate clusters of MT by L-SNCEE.

4.3 S-NITROSOCYSTEINE ETHYL ESTER (SNCEE) ACTIVATES THE cGMP REPORTER, CYGNET-2

SPAEC were transfected with cDNA encoding a fluorescent cGMP indicator (cygnet-2) consisting of cGMP-dependent PKG Iα, minus residues 1–77, bracketed between cyan and yellow mutants of green fluorescent protein (kindly donated by Roger Y. Tsien, University of California at San Diego). cGMP induces conformational changes in PKG Iα, detectable as decreases in FRET between the cyan and the yellow protein with the cygnet-2 reporter [10].

In contrast to the FRET-MT reporter molecule, cygnet-2 responded equally to both the L- and the D-stereoisoforms of SNCEE, with decreases in the FRET ratio of 18.1 ± 3.6 and 17.0 ± 7.0%, respectively (Figure 15 and 10). This decrease in energy transfer was consistent with increases in cGMP, as previously shown with this FRET reporter in response to activation of soluble or particulate guanylyl cyclase by nitric oxide donors or C-type natriuretic peptide, respectively [10]. Furthermore, in contrast to FRET-MT, the scavenging of extracellular ·NO by HbO_2 blocked the L-SNCEE-mediated effects on the cygnet-2 reporter (Figure 16 and 14).

A 10 min pretreatment of cells with 10 μM ODQ (1H-[2 and 4]-oxadiazolo[4,3-α] quinoxalin-1-one), a selective inhibitor of sGC, prevented the SNCEE-mediated changes in energy transfer (mean change in FRET ratio, −1.5 ± 10.4%), demonstrating that these effects were dependent upon activation of sGC and resultant increases in cGMP.

It is believed that S-nitrosothiols activate sGC via decomposition and formation of ·NO [86-88] which interacts with the iron-porphyrin center of the enzyme [89]. There has also been speculation regarding the direct activation of sGC by S-nitrosothiols [84, 90, 91]. Our results,

however, suggest that SNCEE activated PKG Iα via a Fe-nitrosyl heme complex since cGMP production was sensitive to ODQ. Cygnet-2 also responded effectively to the ·NO donor, PAPAnonate (100 μM) with a mean decrease of 13.9 ± 1.2% in energy transfer.

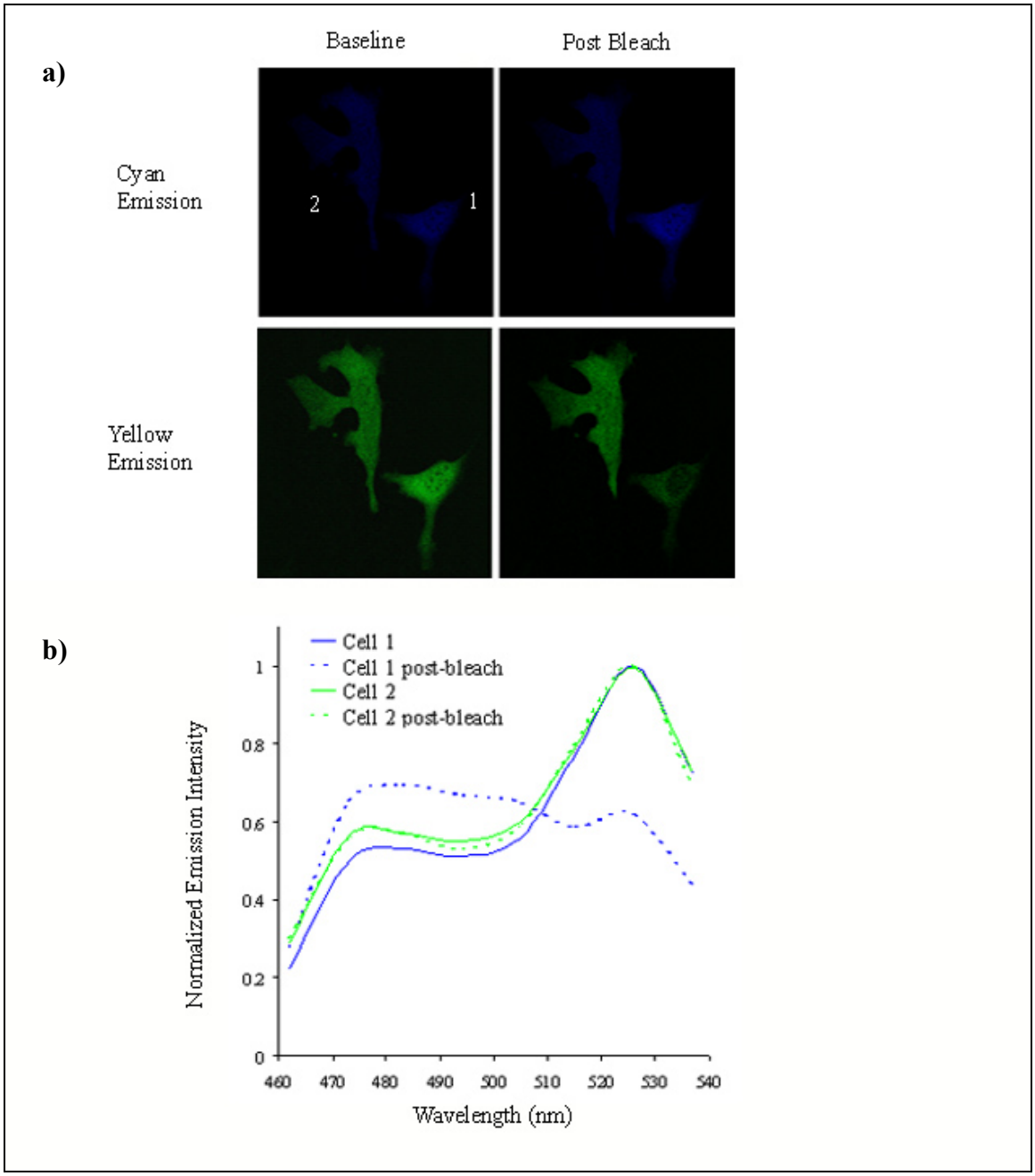

Figure 7 Selective acceptor photobleaching to confirm FRET under baseline conditions. a) Confirmation of energy transfer using acceptor photo-bleaching of the FRET-MT construct. Lung endothelial cells were infected with an adenoviral vector encoding the fluorescent FRET-MT reporter molecule and imaged 24 hours later. Fluorescence resonance energy transfer (FRET) was detected in real time, using full spectral confocal imaging. The images show the separation of the two emitted signals (cyan and yellow) following spectral unmixing based on individual calibration spectra for each protein. b) The graph shows the spectral report provided by the Zeiss software. Following selective photo-bleaching of cell 1, the donor (cyan) was unquenched, resulting in a pronounced increase in the peak emission intensity (~485 nm) indicative of positive FRET. In contrast, there were no changes in the emission intensity of the unbleached cell 2.

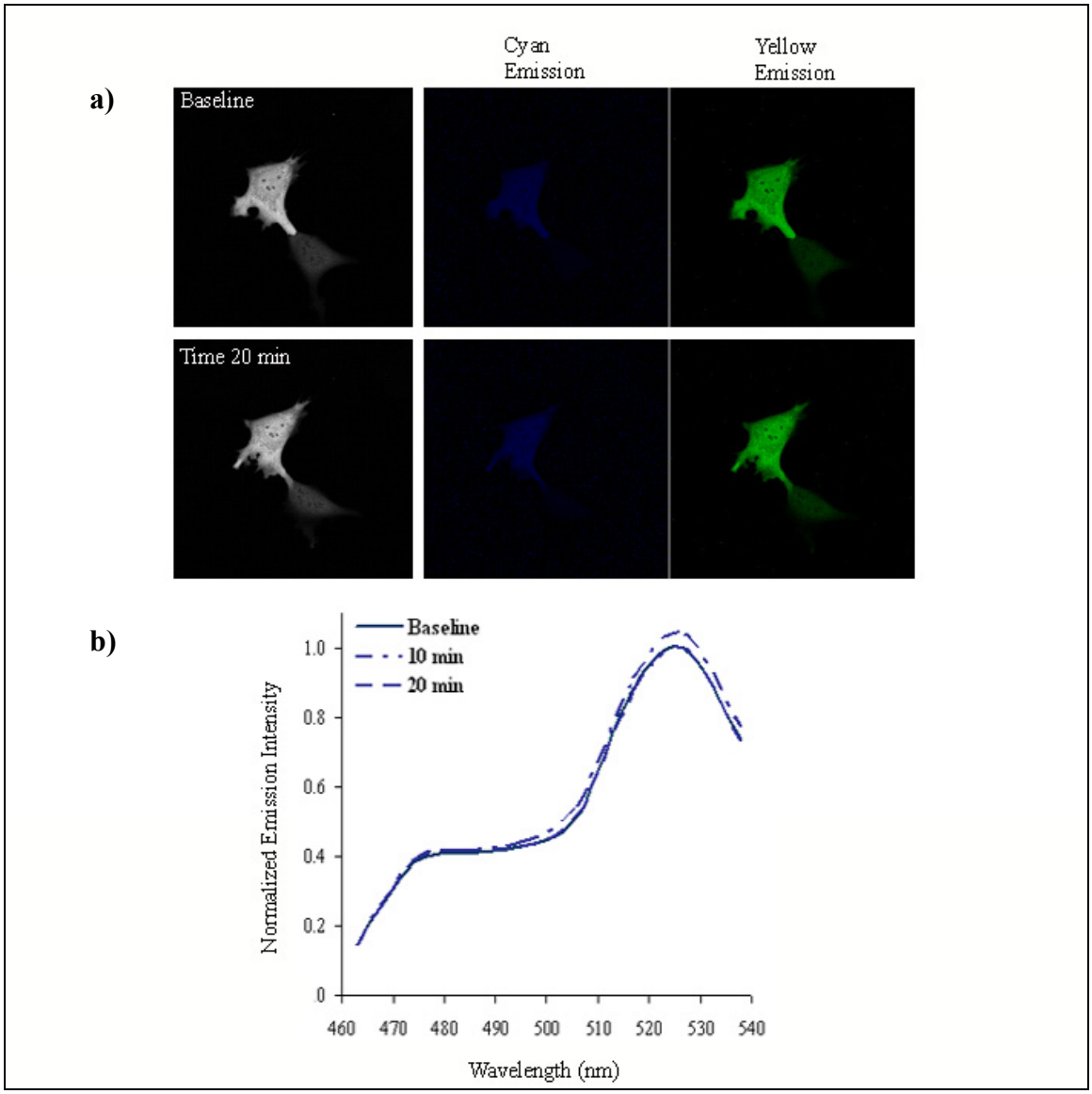

Figure 8 Effects of repeated laser exposure on cyan and yellow emissions. a) Control experiments were performed to determine the effects of repeated laser exposure on the FRET constructs and the calculated FRET ratios. The field of cells shown was exposed to repeated scans using the 458 line of the argon laser and imaged every 2 minutes for 20 minutes. The images of two endothelial cells expressing FRET-MT, shown have undergone linear unmixing using calibration spectra for ECFP and EYFP and therefore represent the separate contributions of the cyan and yellow emissions. b) The spectral report shows that exposing the cells to the 458 line of the argon laser every 2 minutes, over a 20 minute time frame had no effect in the peak emission intensity of the donor (ECFP, ~485nm) nor in that of the acceptor (EYFP, ~525nm) confirming that the observed changes in FRET following SNCEE are not likely due to selective bleaching of the YFP.

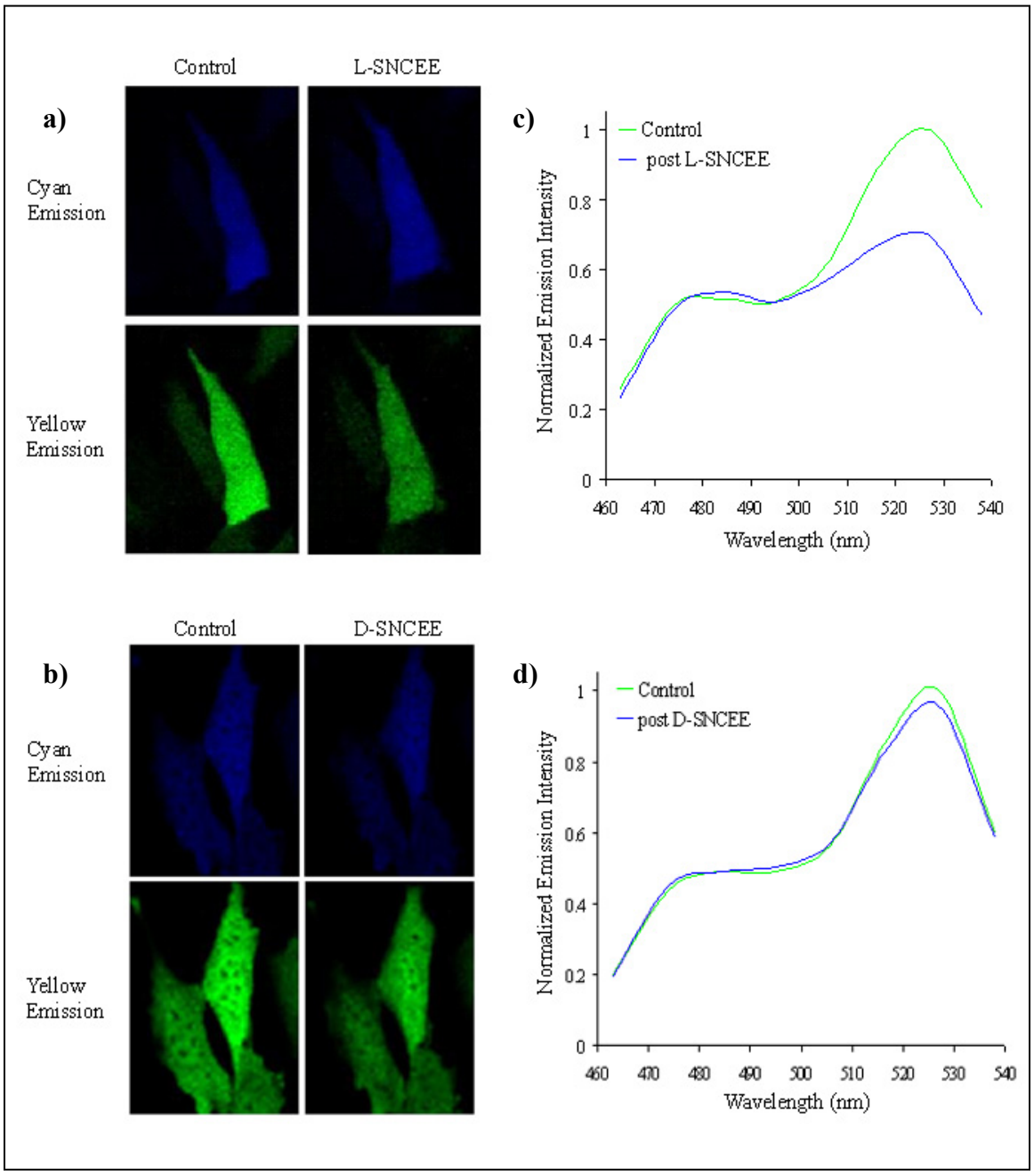

Figure 9 S-nitrosocysteine ethyl ester (SNCEE) activates FRET-MT stereoselectively. a), b) Cyan and yellow emissions at baseline and after application of L- and D- SNCEE, in live endothelial cells that express the FRET-MT reporter. Lung endothelial cells were infected with an adenoviral vector encoding the fluorescent FRET-MT reporter molecule. FRET was detected in real time, using full spectral confocal imaging. The images illustrate the separation of the two emitted signals (cyan and yellow) after spectral unmixing based on individual calibration spectra for each protein. c), d) Spectral report for individual endothelial cells expressing FRET-MT. c) L-SNCEE (50 μM) induced conformational changes in the FRET-MT reporter as shown by a decrease in energy transfer with an increase in the peak emission intensity of the donor (cyan, ~485 nm) and a decrease in that of the acceptor (yellow, ~525 nm). d) D-SNCEE had no appreciable effect on the FRET-MT reporter molecule.

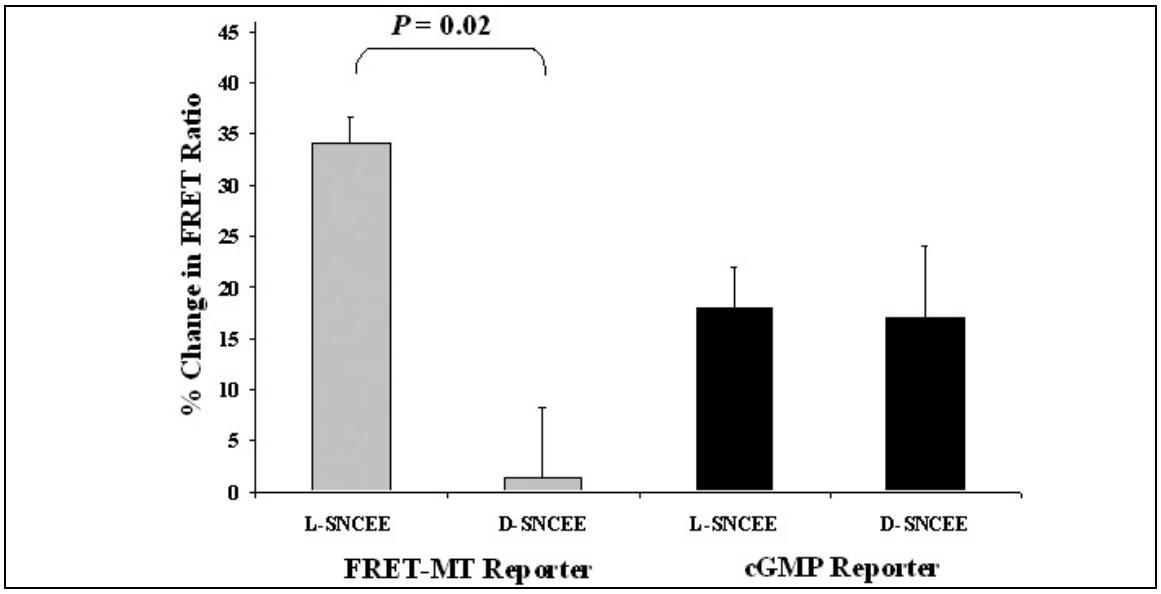

Figure 10 Mean effects of S-nitrosocysteine ethyl ester (SNCEE) on the FRET-MT and cygnet-2 reporters. Mean changes (±SD) in FRET, expressed as a percentage change from control, for both the FRET-MT and cygnet-2 (cGMP) reporter molecules in response to the L- and D-stereoisomers SNCEE. The mean represents three experiments per condition (three to five cells per experiment).

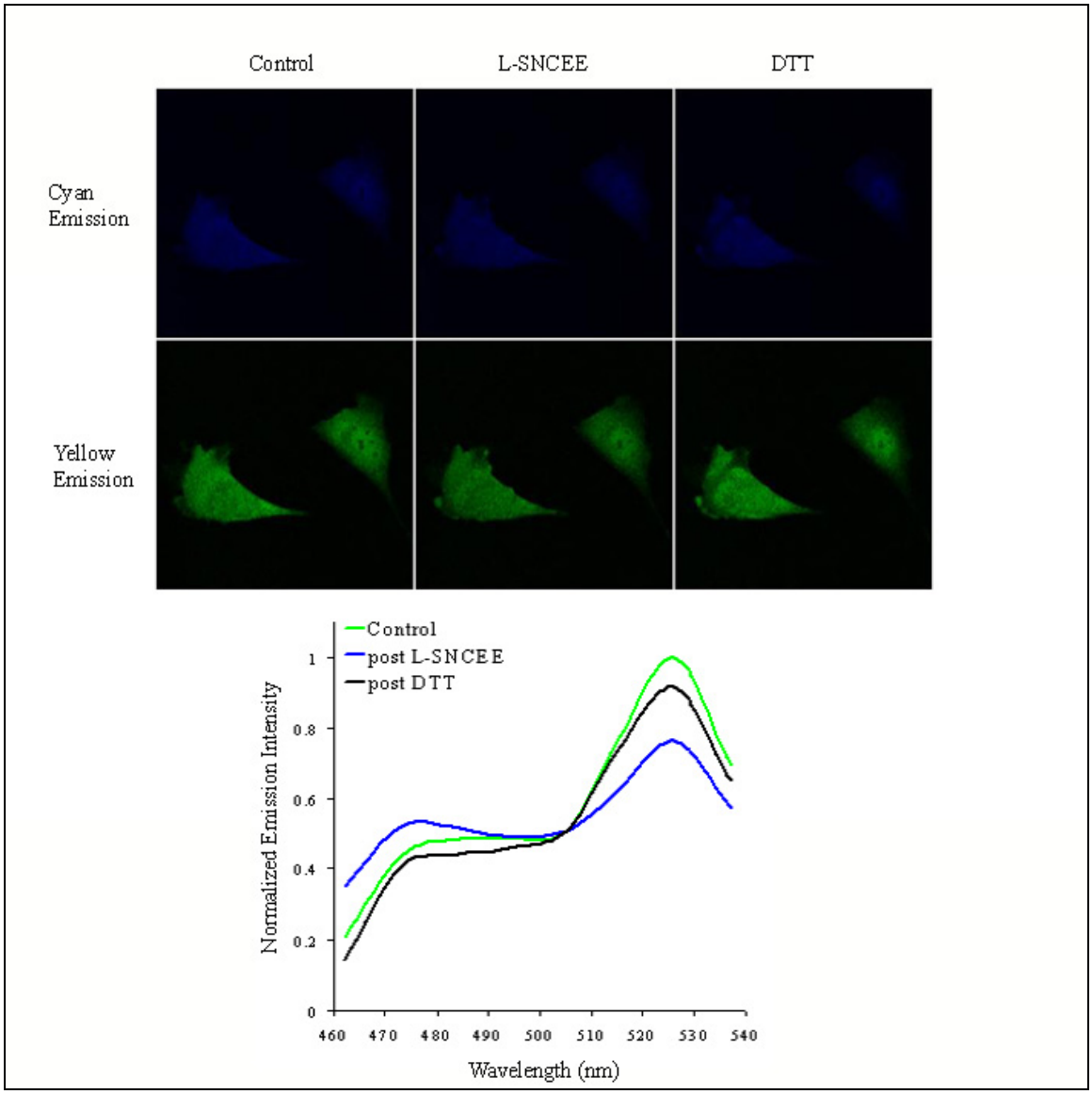

Figure 11 S-nitroso-L-cysteine-EE (L-SNCEE) mediated changes in FRET-MT are reversible. The effects of L-SNCEE on FRET-MT were reversed by dithiothreitol (DTT). As shown by the spectral report from a single cell (bottom), L-SNCEE (50 μM) caused a decrease in the peak emission of the FRET donor (cyan, 458 nm) and an increase in the peak emission of the FRET acceptor (yellow, 525 nm). Application of DTT (50 μM) reversed these effects.

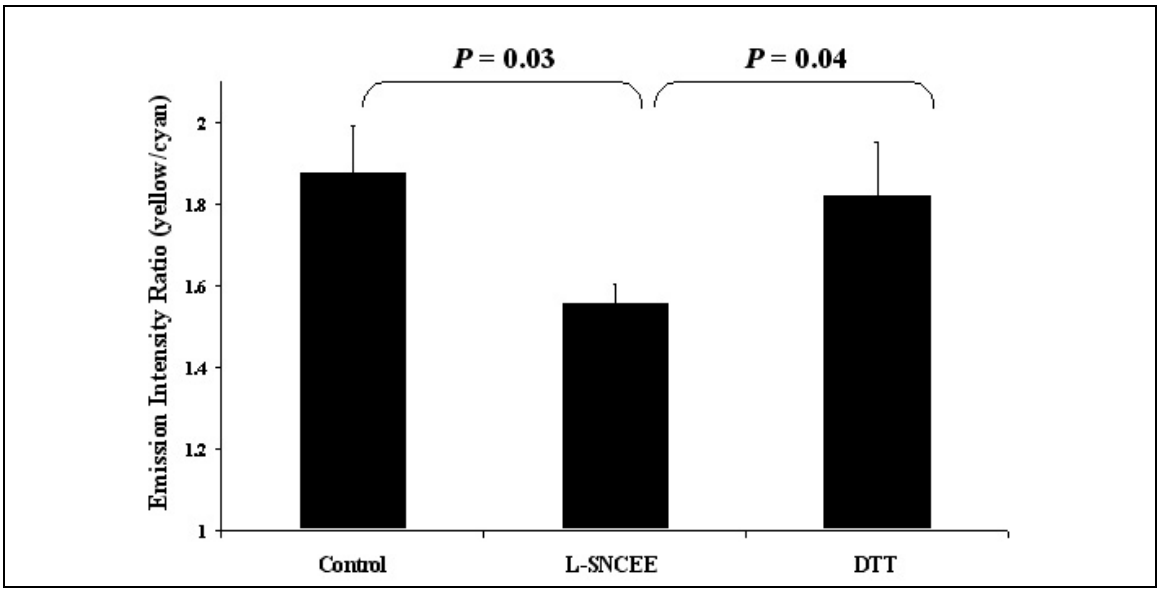

Figure 12 Mean data showing reversibility of S-nitroso-L-cysteine-EE (L-SNCEE) mediated changes in FRET-MT. Mean data from seven cells in three separate experiments showed a significant decrease in FRET ratio (from 1.9 ± 0.1 to 1.5 ± 0.1, $p < .05$) after application of L-SNCEE and an increase in FRET ratio to baseline levels (1.8 ± 0.1, $p > .05$) 6 min after DTT treatment.

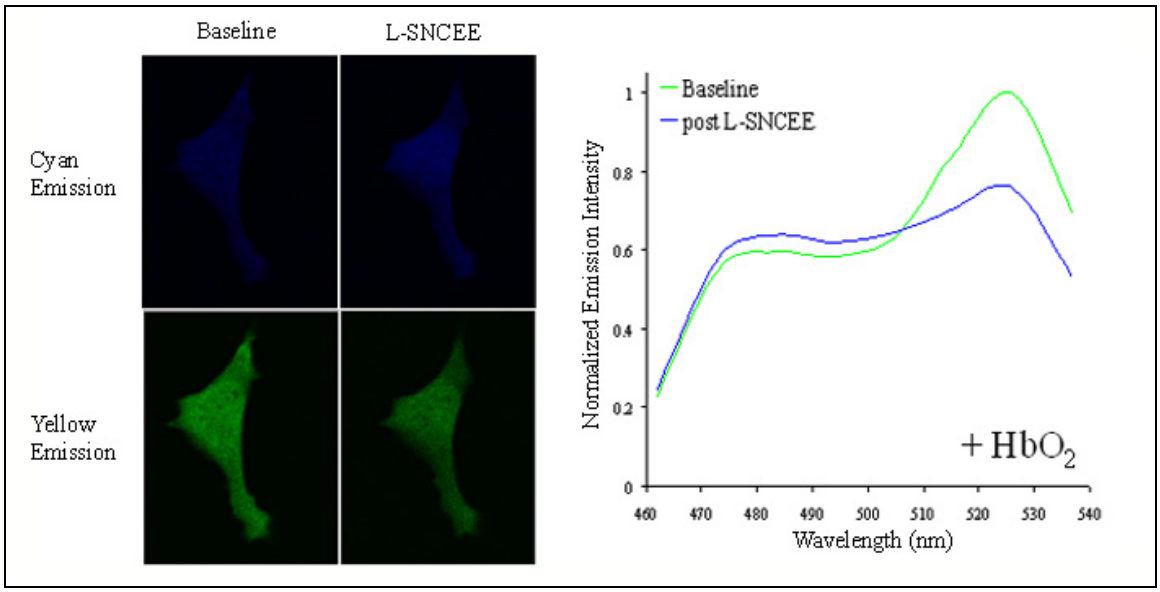

Figure 13 Effects of S-nitroso-L-cysteine-EE (L-SNCEE) on FRET-MT are unaffected by HbO_2 (100 μM). As shown by the spectral report from a single cell (right), even in the presence of HbO_2 (100 μM), L-SNCEE (50 μM) caused change in the peak emission of the FRET acceptor (yellow, 525 nm), and thus a decrease in FRET ratio.

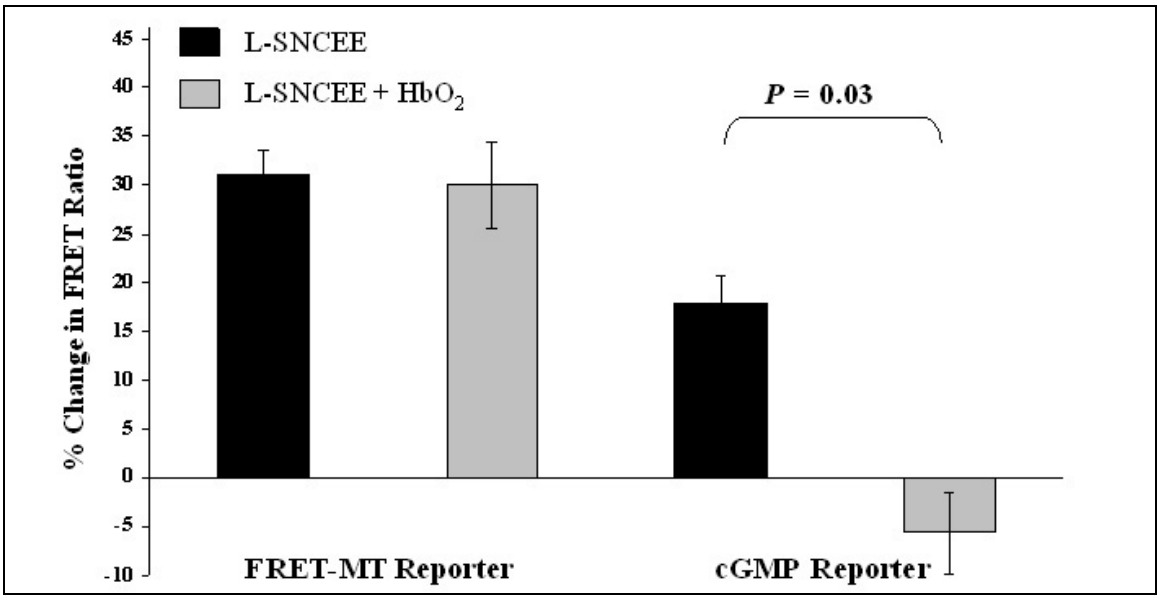

Figure 14 Mean data showing that OxyHemoglobin (HbO_2) prevented L-SNCEE mediated effects in cygnet-2 but did not affect FRET-MT reporter. Mean changes (±SD) in FRET, expressed as a percentage change from control, for both the FRET-MT and cygnet-2 (cGMP) reporter molecules in response to L-SNCEE in the presence or absence of HbO_2 (100 μM). The mean represents three experiments per condition (three to five cells per experiment). For cells expressing FRET-MT, the mean data shows no difference between the 2 conditions. For cells expressing cygnet-2, there is a blunting of the response to L-SNCEE (23.6 ± 2.6, $p < .05$) in presence of HbO_2.

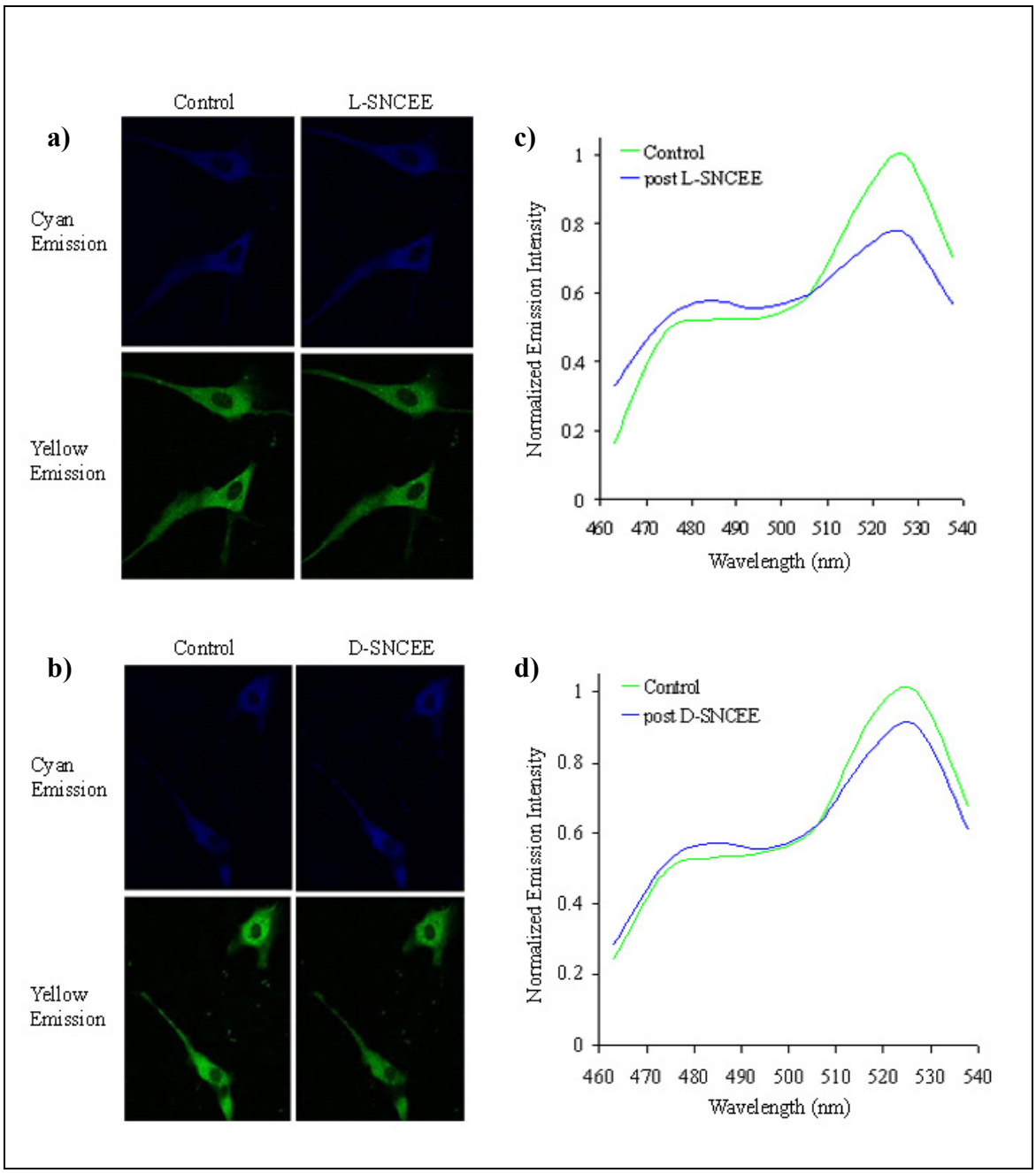

Figure 15 L- and D-isoforms of S-nitrosocysteine ethyl ester (SNCEE) activate the cGMP reporter, cygnet-2. a) and b) Cyan and yellow emissions at baseline and after application of L-SNCEE and D-SNCEE in live endothelial cells that transfected with cygnet-2 reporter. FRET was detected in real time, using full spectral confocal imaging. The images illustrate the separation of the two emitted signals (cyan and yellow) after spectral unmixing based on individual calibration spectra for each protein. c) and d) Spectral reports for individual endothelial cells expressing cygnet-2. Both L-SNCEE (c) and D-SNCEE (d) (50 µM) induced conformational changes in the cygnet-2 (cGMP) reporter as shown by a decrease in energy transfer with an increase in the peak emission intensity of the donor (cyan, ~485 nm) and a decrease in that of the acceptor (yellow, ~525 nm)

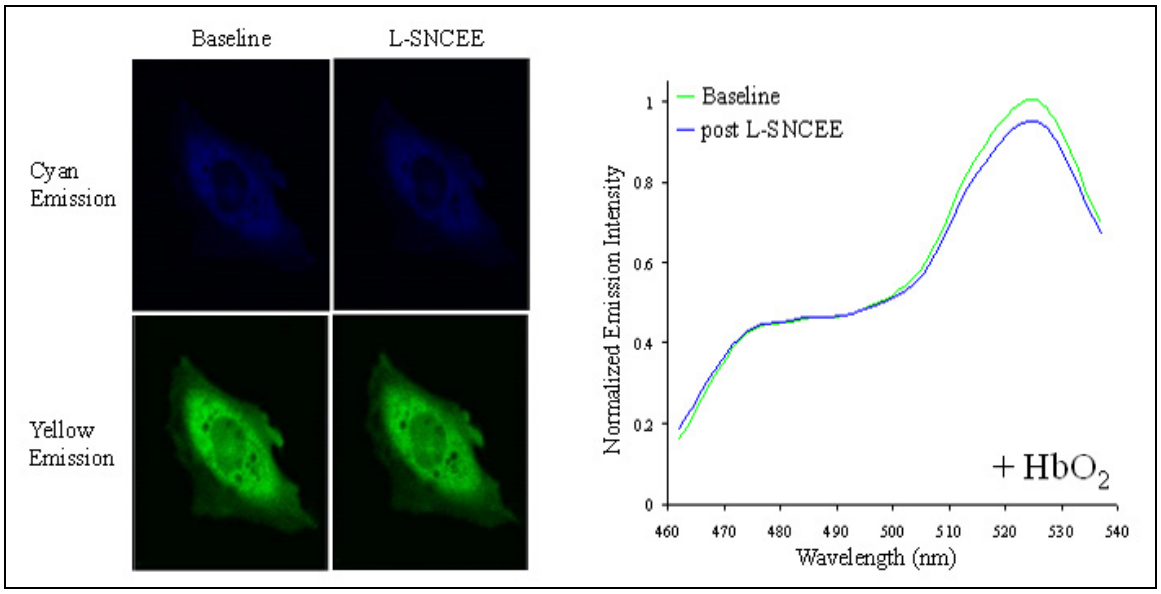

Figure 16 The effects of S-nitroso-L-cysteine-EE (L-SNCEE) on cygnet-2 were affected by oxyhemoglobin (HbO_2). As shown by the spectral report from a single cell (right), L-SNCEE (50 µM) caused no change in the peak emission of the FRET acceptor (yellow, 525 nm). See Figure 14 for mean data.

5.0 DISCUSSION

These results demonstrate that FRET detection using this confocal-based spectral imaging approach is a highly effective technique for detecting post-translation protein modifications induced by NO-related species in live cells. We observed (Figure 9) stereo-specific effects of the membrane permeant forms of the D- and L-isoforms of SNCEE on the FRET-based reporter for MT. D- and L-SNCEE decomposed equally in cell based assays, however, and affected comparable changes in the cGMP reporter, cygnet-2, likely via activation of guanylyl cyclase by formation of a Fe-nitrosyl heme complex (Figure 15). L-SNCEE-induced changes in FRET-MT were reversible by DTT (Figure 11) and insensitive to extracellular oxyhemoglobin (Figure 13). These data corroborate our *in vitro* finding that NO can S-nitrosate MT [92] and provide spectral laser scanning confocal imaging of FRET-based conformational changes in MT, consistent with direct transnitrosation of the protein as previously demonstrated with conventional microscopy [13].

5.1 TRANSNITROSATION OF METALLOTHIONEIN (MT) BY SNCEE

Putative mechanisms governing the stereoselective effects of bolus infusions of S-nitrosocysteine on vascular smooth muscle [93], and on CNS-mediated regulation of cardiovascular [56] and respiratory [55] activities, include stereospecific receptor and/or

transporter interactions and stereoselective catabolism. Indeed the mechanisms governing these physiological effects are likely membrane-based because S-nitrosocysteine (SNC) is an unstable, hydrophilic compound that cannot efficiently cross membranes [78]. Many of the biological effects of exogenous application of SNC may therefore be attributed to its extracellular decomposition to ·NO. In this report, however, we utilized the D- and L-stereoisomers of the lipophilic SNCEE, previously shown to be stable in solutions containing metal chelators and to accumulate inside human neutrophils [78]. The preferential effects of S-nitroso- L-cysteine (L-SNCEE) on FRET-MT therefore might suggest that the structure of the L-stereoisomer of SNCEE confers access to a critical cysteine residue(s) in the metallothionein protein and that the observed changes in energy transfer are via direct transnitrosation of MT. The reversal of L-SNCEE-mediated changes in FRET-MT by dithiothreitol (DTT) provides further support for such nitrosative modifications to a cysteine residue(s) in MT, as DTT is reported to effectively remove thiol-bound NO groups from proteins [94, 95]. Alternatively, our methodology does not allow us to eliminate the possibility that a stereoselective amino acid transport system, such as that recently described for SNC in PC12 cells [96], may also contribute to the differing effects of L- and D-SNCEE on FRET-MT.

We showed previously that FRET-MT was sensitive to bolus additions of buffer saturated with NO gas [13], whereas the present results show that ·NO liberated from D-SNCEE had no effect on this construct. The apparent discrepancy is most likely explained by exposure of the cells to much higher ·NO concentrations in these earlier reports, which, under aerobic conditions, can form reactive species capable of nitrosating MT [97]. These conclusions are supported by the *in vitro* data demonstrating the S-nitrosation of purified MT protein in the presence of NO donors [92]. In summary, the collective evidence suggests that L-SNCEE alters the

conformation of FRET-MT via transnitrosation of MT cysteine(s); however, our evidence for S-nitrosation remains indirect and it is therefore possible that an alternative DTT-reversible mechanism could explain these effects.

Nitrosothiol-induced conformational changes in FRET-MT are consistent with previous reports both by our group [14, 92] and by others [39, 61] of NO-mediated release of metals from the thiolate clusters of metallothionein. The recent development of a FRET-based nanosensor based on the β-domain of recombinant metallothionein [98] may be useful in providing detailed structural information and quantification of zinc binding and release by the reportedly more reactive [99, 100] of the two metal binding domains of MT in response to NO-related species. Unlike the genetically encoded GFP-based probes, however, introduction of this fluorescently labeled FRET indicator [98] into living cells will require microinjection techniques and as yet remains untested.

5.2 ACTIVATION OF THE cGMP REPORTER, CYGNET-2 BY SNCEE

It is believed that S-nitrosothiols activate sGC via decomposition and formation of ·NO [86-88], which interacts with the iron–porphyrin center of the enzyme [89]. There has also been speculation regarding the direct activation of sGC by S-nitrosothiols [84, 90]. Our results, however, suggest that SNCEE activated PKG Iα via an Fe–nitrosyl heme complex because cGMP production was sensitive to ODQ, which oxidizes the ferrous form of sGC to the ferric species and irreversibly inactivates the enzyme [101]. Furthermore, the scavenging of extracellular ·NO by HbO_2 blocked the L-SNCEE-mediated effects on the cygnet-2 reporter. It should be noted that the concentration of SNCEE (50 μM) used in these experiments may

generate ·NO concentrations that are in excess of the reported EC50 for sGC, which ranges from 1 to 400 nM dependent upon the method of NO delivery [102]. If this is the case, then sGC could be maximally activated by only a small percentage of the total liberated ·NO, and differences in the decomposition of L- versus D-SNCEE would not be detectable using our PKG-based FRET reporter. Pertinent to this discussion is the possibility that transnitrosation of MT occurs via breakdown of SNCEE and autoxidation of ·NO. This chemistry will exhibit second-order dependence on the free [·NO], thus amplifying even modest differences in breakdown of L- versus D-SNCEE. However, our indirect determinations of ·NO using the Griess reaction to measure the stable decomposition products, NO_3^- and NO_2^-, indicate that L- and D-SNCEE generate equivalent amounts of ·NO under our experimental conditions.

5.3 FRET DETECTION

FRET between GFP mutants offers a general mechanism to build genetically encoded indicators and to monitor dynamic molecular interactions in living systems. This report describes the use of spectral confocal-based imaging for FRET detection that is capable of providing full spectral information for each voxel of the fluorescent image. This obviates problems of signal bleedthrough and channel cross talk and permits detection of small, but potentially biologically meaningful, changes in FRET that are extremely difficult to resolve reliably using the more traditional methods relying on band-pass filters. It also allows the use of more efficient pair of donor and acceptor fluorophore pairs for FRET imaging. We found that FRET detection using this spectral imaging approach is a highly effective technique for detecting post-translation protein modifications induced by NO-related species in living cells.

5.4 FUTURE DIRECTION

In this study we have demonstrated the use of full spectral fluorescence resonance energy transfer (FRET) in detecting NO signaling events including transnitrosation of metallothionein and S-nitrosylation (guanylyl cyclase) in live pulmonary endothelial cells.

The next challenge is to visualize these NO-based signaling events in *in situ*. To this end, we have recently had success in targeting the FRET-MT reporter construct to the pulmonary endothelium of mice using tail vein injection of DOTAP-cationic liposomes followed by an adenovirus containing cDNA for FRET-MT. Using an isolated, perfused lung preparation we found that the FRET-MT construct was functional in the intact organ and was sensitive to the addition of NO donors to the perfusion circuit.

BIBLIOGRAPHY

[1] Gaston, B. (1999) Nitric oxide and thiol groups *Biochim Biophys Acta* **1411,** 323-33.

[2] Stamler, J. S., Singel, D. J., and Loscalzo, J. (1992) Biochemistry of nitric oxide and its redox-activated forms *Science* **258,** 1898-902.

[3] Kuppusamy, P., Wang, P., Samouilov, A., and Zweier, J. L. (1996) Spatial mapping of nitric oxide generation in the ischemic heart using electron paramagnetic resonance imaging *Magn Reson Med* **36,** 212-8.

[4] Kojima, H., Hirata, M., Kudo, Y., Kikuchi, K., and Nagano, T. (2001) Visualization of oxygen-concentration-dependent production of nitric oxide in rat hippocampal slices during aglycemia *J Neurochem* **76,** 1404-10.

[5] Kojima, H., Nakatsubo, N., Kikuchi, K., Kawahara, S., Kirino, Y., Nagoshi, H., Hirata, Y., and Nagano, T. (1998) Detection and imaging of nitric oxide with novel fluorescent indicators: diaminofluoresceins *Anal Chem* **70,** 2446-53.

[6] Jourd'heuil, D. (2002) Increased nitric oxide-dependent nitrosylation of 4,5-diaminofluorescein by oxidants: implications for the measurement of intracellular nitric oxide *Free Radic Biol Med* **33,** 676-84.

[7] Zhang, X., Kim, W. S., Hatcher, N., Potgieter, K., Moroz, L. L., Gillette, R., and Sweedler, J. V. (2002) Interfering with nitric oxide measurements. 4,5-diaminofluorescein reacts with dehydroascorbic acid and ascorbic acid *J Biol Chem* **277,** 48472-8.

[8] Broillet, M., Randin, O., and Chatton, J. (2001) Photoactivation and calcium sensitivity of the fluorescent NO indicator 4,5-diaminofluorescein (DAF-2): implications for cellular NO imaging *FEBS Lett* **491,** 227-32.

[9] Miyawaki, A., Llopis, J., Heim, R., McCaffery, J. M., Adams, J. A., Ikura, M., and Tsien, R. Y. (1997) Fluorescent indicators for Ca2+ based on green fluorescent proteins and calmodulin *Nature* **388,** 882-7.

[10] Honda, A., Adams, S. R., Sawyer, C. L., Lev-Ram, V., Tsien, R. Y., and Dostmann, W. R. (2001) Spatiotemporal dynamics of guanosine 3',5'-cyclic monophosphate revealed by a genetically encoded, fluorescent indicator *Proc Natl Acad Sci U S A* **98,** 2437-42.

[11] Zaccolo, M., De Giorgi, F., Cho, C. Y., Feng, L., Knapp, T., Negulescu, P. A., Taylor, S. S., Tsien, R. Y., and Pozzan, T. (2000) A genetically encoded, fluorescent indicator for cyclic AMP in living cells *Nat Cell Biol* **2,** 25-9.

[12] Ting, A. Y., Kain, K. H., Klemke, R. L., and Tsien, R. Y. (2001) Genetically encoded fluorescent reporters of protein tyrosine kinase activities in living cells *Proc Natl Acad Sci U S A* **98,** 15003-8.

[13] Pearce, L. L., Gandley, R. E., Han, W., Wasserloos, K., Stitt, M., Kanai, A. J., McLaughlin, M. K., Pitt, B. R., and Levitan, E. S. (2000) Role of metallothionein in nitric oxide signaling as revealed by a green fluorescent fusion protein *Proc Natl Acad Sci U S A* **97,** 477-82.

[14] St Croix, C. M., Wasserloos, K. J., Dineley, K. E., Reynolds, I. J., Levitan, E. S., and Pitt, B. R. (2002) Nitric oxide-induced changes in intracellular zinc homeostasis are mediated by metallothionein/thionein *Am J Physiol Lung Cell Mol Physiol* **282,** L185-92.

[15] Lancaster, J. R., Jr. (1997) A tutorial on the diffusibility and reactivity of free nitric oxide *Nitric Oxide* **1,** 18-30.

[16] Gow, A. J., and Ischiropoulos, H. (2001) Nitric oxide chemistry and cellular signaling *J Cell Physiol* **187,** 277-82.

[17] Davis, K. L., Martin, E., Turko, I. V., and Murad, F. (2001) Novel effects of nitric oxide *Annu Rev Pharmacol Toxicol* **41,** 203-36.

[18] Rairigh, R. L., Storme, L., Parker, T. A., le Cras, T. D., Kinsella, J. P., Jakkula, M., and Abman, S. H. (1999) Inducible NO synthase inhibition attenuates shear stress-induced pulmonary vasodilation in the ovine fetus *Am J Physiol* **276,** L513-21.

[19] Sessa, W. C., Pritchard, K., Seyedi, N., Wang, J., and Hintze, T. H. (1994) Chronic exercise in dogs increases coronary vascular nitric oxide production and endothelial cell nitric oxide synthase gene expression *Circ Res* **74,** 349-53.

[20] Arnal, J. F., Yamin, J., Dockery, S., and Harrison, D. G. (1994) Regulation of endothelial nitric oxide synthase mRNA, protein, and activity during cell growth *Am J Physiol* **267,** C1381-8.

[21] Le Cras, T. D., and McMurtry, I. F. (2001) Nitric oxide production in the hypoxic lung *Am J Physiol Lung Cell Mol Physiol* **280,** L575-82.

[22] Rubanyi, G. M., Romero, J. C., and Vanhoutte, P. M. (1986) Flow-induced release of endothelium-derived relaxing factor *Am J Physiol* **250,** H1145-9.

[23] Kuchan, M. J., Jo, H., and Frangos, J. A. (1994) Role of G proteins in shear stress-mediated nitric oxide production by endothelial cells *Am J Physiol* **267,** C753-8.

[24] Rizzo, V., McIntosh, D. P., Oh, P., and Schnitzer, J. E. (1998) *In situ* flow activates endothelial nitric oxide synthase in luminal caveolae of endothelium with rapid caveolin dissociation and calmodulin association *J Biol Chem* **273,** 34724-9.

[25] Arnal, J. F., Dinh-Xuan, A. T., Pueyo, M., Darblade, B., and Rami, J. (1999) Endothelium-derived nitric oxide and vascular physiology and pathology *Cell Mol Life Sci* **55,** 1078-87.

[26] Corson, M. A., James, N. L., Latta, S. E., Nerem, R. M., Berk, B. C., and Harrison, D. G. (1996) Phosphorylation of endothelial nitric oxide synthase in response to fluid shear stress *Circ Res* **79,** 984-91.

[27] Dimmeler, S., Fleming, I., Fisslthaler, B., Hermann, C., Busse, R., and Zeiher, A. M. (1999) Activation of nitric oxide synthase in endothelial cells by Akt-dependent phosphorylation *Nature* **399,** 601-5.

[28] Lowenstein, C. J., Dinerman, J. L., and Snyder, S. H. (1994) Nitric oxide: a physiologic messenger *Ann Intern Med* **120,** 227-37.

[29] Murad, F. (1996) The 1996 Albert Lasker Medical Research Awards. Signal transduction using nitric oxide and cyclic guanosine monophosphate *Jama* **276,** 1189-92.

[30] Dawson, T. M., Dawson, V. L., and Snyder, S. H. (1992) A novel neuronal messenger molecule in brain: the free radical, nitric oxide *Ann Neurol* **32,** 297-311.

[31] Lipton, S. A. (1999) Neuronal protection and destruction by NO *Cell Death Differ* **6,** 943-51.

[32] Hibbs, J. B., Jr., Taintor, R. R., Vavrin, Z., and Rachlin, E. M. (1988) Nitric oxide: a cytotoxic activated macrophage effector molecule *Biochem Biophys Res Commun* **157,** 87-94.

[33] Kobayashi, O., Miwa, H., Watanabe, S., Tsujii, M., Dubois, R. N., and Sato, N. (2001) Cyclooxygenase-2 downregulates inducible nitric oxide synthase in rat intestinal epithelial cells *Am J Physiol Gastrointest Liver Physiol* **281,** G688-96.

[34] Salvemini, D., Misko, T. P., Masferrer, J. L., Seibert, K., Currie, M. G., and Needleman, P. (1993) Nitric oxide activates cyclooxygenase enzymes *Proc Natl Acad Sci U S A* **90,** 7240-4.

[35] Marletta, M. A. (1989) Nitric oxide: biosynthesis and biological significance *Trends Biochem Sci* **14,** 488-92.

[36] Wink, D. A., and Mitchell, J. B. (1998) Chemical biology of nitric oxide: Insights into regulatory, cytotoxic, and cytoprotective mechanisms of nitric oxide *Free Radic Biol Med* **25,** 434-56.

[37] Lucas, K. A., Pitari, G. M., Kazerounian, S., Ruiz-Stewart, I., Park, J., Schulz, S., Chepenik, K. P., and Waldman, S. A. (2000) Guanylyl cyclases and signaling by cyclic GMP *Pharmacol Rev* **52,** 375-414.

[38] Kwan, H. Y., Huang, Y., and Yao, X. (2000) Store-operated calcium entry in vascular endothelial cells is inhibited by cGMP via a protein kinase G-dependent mechanism *J Biol Chem* **275,** 6758-63.

[39] Kroncke, K. D., Fehsel, K., Schmidt, T., Zenke, F. T., Dasting, I., Wesener, J. R., Bettermann, H., Breunig, K. D., and Kolb-Bachofen, V. (1994) Nitric oxide destroys zinc-sulfur clusters inducing zinc release from metallothionein and inhibition of the zinc finger-type yeast transcription activator LAC9 *Biochem Biophys Res Commun* **200,** 1105-10.

[40] Kroncke, K. D., and Carlberg, C. (2000) Inactivation of zinc finger transcription factors provides a mechanism for a gene regulatory role of nitric oxide *Faseb J* **14,** 166-73.

[41] Berendji, D., Kolb-Bachofen, V., Zipfel, P. F., Skerka, C., Carlberg, C., and Kroncke, K. D. (1999) Zinc finger transcription factors as molecular targets for nitric oxide-mediated immunosuppression: inhibition of IL-2 gene expression in murine lymphocytes *Mol Med* **5,** 721-30.

[42] Kroncke, K. D. (2001) Cysteine-Zn2+ complexes: unique molecular switches for inducible nitric oxide synthase-derived NO *Faseb J* **15,** 2503-7.

[43] Kroncke, K. D., and Kolb-Bachofen, V. (1999) Measurement of nitric oxide-mediated effects on zinc homeostasis and zinc finger transcription factors *Methods Enzymol* **301,** 126-35.

[44] Radi, R., Beckman, J. S., Bush, K. M., and Freeman, B. A. (1991) Peroxynitrite oxidation of sulfhydryls. The cytotoxic potential of superoxide and nitric oxide *J Biol Chem* **266,** 4244-50.

[45] Szabo, C., and Ohshima, H. (1997) DNA damage induced by peroxynitrite: subsequent biological effects *Nitric Oxide* **1,** 373-85.

[46] Rubbo, H., Radi, R., Trujillo, M., Telleri, R., Kalyanaraman, B., Barnes, S., Kirk, M., and Freeman, B. A. (1994) Nitric oxide regulation of superoxide and peroxynitrite-dependent lipid peroxidation. Formation of novel nitrogen-containing oxidized lipid derivatives *J Biol Chem* **269,** 26066-75.

[47] Williams, D. L. (2003) A chemist's view of the nitric oxide story *Org Biomol Chem* **1,** 441-9.

[48] Kharitonov, V. G., Sundquist, A. R., and Sharma, V. S. (1995) Kinetics of nitrosation of thiols by nitric oxide in the presence of oxygen *J Biol Chem* **270,** 28158-64.

[49] Mallis, R. J., and Thomas, J. A. (2000) Effect of S-nitrosothiols on cellular glutathione and reactive protein sulfhydryls *Arch Biochem Biophys* **383,** 60-9.

[50] Stamler, J. S. (1995) S-nitrosothiols and the bioregulatory actions of nitrogen oxides through reactions with thiol groups *Curr Top Microbiol Immunol* **196,** 19-36.

[51] Stamler, J. S., Lamas, S., and Fang, F. C. (2001) Nitrosylation. the prototypic redox-based signaling mechanism *Cell* **106,** 675-83.

[52] Xu, L., Eu, J. P., Meissner, G., and Stamler, J. S. (1998) Activation of the cardiac calcium release channel (ryanodine receptor) by poly-S-nitrosylation *Science* **279,** 234-7.

[53] Lei, S. Z., Pan, Z. H., Aggarwal, S. K., Chen, H. S., Hartman, J., Sucher, N. J., and Lipton, S. A. (1992) Effect of nitric oxide production on the redox modulatory site of the NMDA receptor-channel complex *Neuron* **8,** 1087-99.

[54] Mannick, J. B., Hausladen, A., Liu, L., Hess, D. T., Zeng, M., Miao, Q. X., Kane, L. S., Gow, A. J., and Stamler, J. S. (1999) Fas-induced caspase denitrosylation *Science* **284,** 651-4.

[55] Lipton, A. J., Johnson, M. A., Macdonald, T., Lieberman, M. W., Gozal, D., and Gaston, B. (2001) S-nitrosothiols signal the ventilatory response to hypoxia *Nature* **413,** 171-4.

[56] Ohta, H., Bates, J. N., Lewis, S. J., and Talman, W. T. (1997) Actions of S-nitrosocysteine in the nucleus tractus solitarii are unrelated to release of nitric oxide *Brain Res* **746,** 98-104.

[57] Schwarz, M. A., Lazo, J. S., Yalowich, J. C., Allen, W. P., Whitmore, M., Bergonia, H. A., Tzeng, E., Billiar, T. R., Robbins, P. D., Lancaster, J. R., Jr., and et al. (1995) Metallothionein protects against the cytotoxic and DNA-damaging effects of nitric oxide *Proc Natl Acad Sci U S A* **92,** 4452-6.

[58] Pearce, L. L., Wasserloos, K., St Croix, C. M., Gandley, R., Levitan, E. S., and Pitt, B. R. (2000) Metallothionein, nitric oxide and zinc homeostasis in vascular endothelial cells *J Nutr* **130,** 1467S-70S.

[59] Maret, W. (2000) The function of zinc metallothionein: a link between cellular zinc and redox state *J Nutr* **130,** 1455S-8S.

[60] Kawai, K., Liu, S. X., Tyurin, V. A., Tyurina, Y. Y., Borisenko, G. G., Jiang, J. F., St Croix, C. M., Fabisiak, J. P., Pitt, B. R., and Kagan, V. E. (2000) Antioxidant and antiapoptotic function of metallothioneins in HL-60 cells challenged with copper nitrilotriacetate *Chem Res Toxicol* **13,** 1275-86.

[61] Misra, R. R., Hochadel, J. F., Smith, G. T., Cook, J. C., Waalkes, M. P., and Wink, D. A. (1996) Evidence that nitric oxide enhances cadmium toxicity by displacing the metal from metallothionein *Chem Res Toxicol* **9,** 326-32.

[62] Foster, M. W., McMahon, T. J., and Stamler, J. S. (2003) S-nitrosylation in health and disease *Trends Mol Med* **9,** 160-8.

[63] Gladwin, M. T., Wang, X., Reiter, C. D., Yang, B. K., Vivas, E. X., Bonaventura, C., and Schechter, A. N. (2002) S-Nitrosohemoglobin is unstable in the reductive erythrocyte environment and lacks O2/NO-linked allosteric function *J Biol Chem* **277,** 27818-28.

[64] Kelm, M., Dahmann, R., Wink, D., and Feelisch, M. (1997) The nitric oxide/superoxide assay. Insights into the biological chemistry of the NO/O-2. interaction *J Biol Chem* **272,** 9922-32.

[65] Archer, S. (1993) Measurement of nitric oxide in biological models *Faseb J* **7,** 349-60.

[66] Gow, A. J., Luchsinger, B. P., Pawloski, J. R., Singel, D. J., and Stamler, J. S. (1999) The oxyhemoglobin reaction of nitric oxide *Proc Natl Acad Sci U S A* **96,** 9027-32.

[67] Hobbs, A. J., Gladwin, M. T., Patel, R. P., Williams, D. L., and Butler, A. R. (2002) Haemoglobin: NO transporter, NO inactivator or NOne of the above? *Trends Pharmacol Sci* **23,** 406-11.

[68] Itoh, Y., Ma, F. H., Hoshi, H., Oka, M., Noda, K., Ukai, Y., Kojima, H., Nagano, T., and Toda, N. (2000) Determination and bioimaging method for nitric oxide in biological specimens by diaminofluorescein fluorometry *Anal Biochem* **287,** 203-9.

[69] Kojima, H., Urano, Y., Kikuchi, K., Higuchi, T., Hirata, Y., and Nagano, T. (1999) Fluorescent Indicators for Imaging Nitric Oxide Production *Angew Chem Int Ed Engl* **38,** 3209-12.

[70] Tsien, R. Y. (1998) The green fluorescent protein *Annu Rev Biochem* **67,** 509-44.

[71] Gordon, G. W., Berry, G., Liang, X. H., Levine, B., and Herman, B. (1998) Quantitative fluorescence resonance energy transfer measurements using fluorescence microscopy *Biophys J* **74,** 2702-13.

[72] Zaccolo, M. (2004) Use of chimeric fluorescent proteins and fluorescence resonance energy transfer to monitor cellular responses *Circ Res* **94,** 866-73.

[73] Karpova, T. S., Baumann, C. T., He, L., Wu, X., Grammer, A., Lipsky, P., Hager, G. L., and McNally, J. G. (2003) Fluorescence resonance energy transfer from cyan to yellow fluorescent protein detected by acceptor photobleaching using confocal microscopy and a single laser *J Microsc* **209,** 56-70.

[74] Hoyt, D. G., Mannix, R. J., Rusnak, J. M., Pitt, B. R., and Lazo, J. S. (1995) Collagen is a survival factor against LPS-induced apoptosis in cultured sheep pulmonary artery endothelial cells *Am J Physiol* **269,** L171-7.

[75] Carley, W. W., Niedbala, M. J., and Gerritsen, M. E. (1992) Isolation, cultivation, and partial characterization of microvascular endothelium derived from human lung *Am J Respir Cell Mol Biol* **7,** 620-30.

[76] Sciavolino, P. J., Lee, T. H., and Vilcek, J. (1992) Overexpression of metallothionein confers resistance to the cytotoxic effect of TNF with cadmium in MCF-7 breast carcinoma cells *Lymphokine Cytokine Res* **11,** 265-70.

[77] Graham, F. L., and Prevec, L. (1991) Methods in Molecular Biology: Gene Transfer and Expression Protocols, Humana, Clifton, NJ.

[78] Clancy, R., Cederbaum, A. I., and Stoyanovsky, D. A. (2001) Preparation and properties of S-nitroso-L-cysteine ethyl ester, an intracellular nitrosating agent *J Med Chem* **44,** 2035-8.

[79] Baldwin, J. E., Freeman, R. T., Lowe, C., Schofield, C. J., and Lee, E. (1989) A Y-lactam analogue of the penems possessing antibacterial activity *Tetrahedron* **45,** 4537-50.

[80] Eyer, P., and Podhradsky, D. (1986) Evaluation of the micromethod for determination of glutathione using enzymatic cycling and Ellman's reagent *Anal Biochem* **153,** 57-66.

[81] Green, L. C., Wagner, D. A., Glogowski, J., Skipper, P. L., Wishnok, J. S., and Tannenbaum, S. R. (1982) Analysis of nitrate, nitrite, and [15N]nitrate in biological fluids *Anal Biochem* **126,** 131-8.

[82] Bernard, R. (1999) Fundamentals of Biostatistics, Duxbury Press, CA.

[83] St Croix, C. M., Stitt, M. S., Leelavanichkul, K., Wasserloos, K. J., Pitt, B. R., and Watkins, S. C. (2004) Nitric oxide-induced modification of protein thiolate clusters as determined by spectral fluorescence resonance energy transfer in live endothelial cells *Free Radic Biol Med* **37,** 785-92.

[84] Tseng, C. M., Tabrizi-Fard, M. A., and Fung, H. L. (2000) Differential sensitivity among nitric oxide donors toward ODQ-mediated inhibition of vascular relaxation *J Pharmacol Exp Ther* **292,** 737-42.

[85] Tabrizi-Fard, M. A., Lee, W. I., and Fung, H. L. (1999) Differential interactions of nitric oxide donors with rat oxyhemoglobin *Biochem Pharmacol* **58,** 671-4.

[86] Denninger, J. W., and Marletta, M. A. (1999) Guanylate cyclase and the .NO/cGMP signaling pathway *Biochim Biophys Acta* **1411,** 334-50.

[87] Dierks, E. A., and Burstyn, J. N. (1996) Nitric oxide (NO), the only nitrogen monoxide redox form capable of activating soluble guanylyl cyclase *Biochem Pharmacol* **51,** 1593-600.

[88] Napoli, C., and Ignarro, L. J. (2003) Nitric oxide-releasing drugs *Annu Rev Pharmacol Toxicol* **43,** 97-123.

[89] Stone, J. R., and Marletta, M. A. (1994) Soluble guanylate cyclase from bovine lung: activation with nitric oxide and carbon monoxide and spectral characterization of the ferrous and ferric states *Biochemistry* **33,** 5636-40.

[90] Haj-Yehia, A. I., and Benet, L. Z. (1996) *In vivo* depletion of free thiols does not account for nitroglycerin-induced tolerance: a thiol-nitrate interaction hypothesis as an alternative explanation for nitroglycerin activity and tolerance *J Pharmacol Exp Ther* **278,** 1296-305.

[91] Stamler, J. S., Simon, D. I., Osborne, J. A., Mullins, M. E., Jaraki, O., Michel, T., Singel, D. J., and Loscalzo, J. (1992) S-nitrosylation of proteins with nitric oxide: synthesis and characterization of biologically active compounds *Proc Natl Acad Sci U S A* **89,** 444-8.

[92] Liu, S., Kawai, K., Tyurin, V. A., Tyurina, Y. Y., Borisenko, G. G., Fabisiak, J. P., Quinn, P. J., Pitt, B. R., and Kagan, V. E. (2001) Nitric oxide-dependent pro-oxidant and pro-apoptotic effect of metallothioneins in HL-60 cells challenged with cupric nitrilotriacetate *Biochem J* **354,** 397-406.

[93] Davisson, R. L., Travis, M. D., Bates, J. N., and Lewis, S. J. (1996) Hemodynamic effects of L- and D-S-nitrosocysteine in the rat. Stereoselective S-nitrosothiol recognition sites *Circ Res* **79,** 256-62.

[94] Kim, Y. M., Talanian, R. V., and Billiar, T. R. (1997) Nitric oxide inhibits apoptosis by preventing increases in caspase-3-like activity via two distinct mechanisms *J Biol Chem* **272,** 31138-48.

[95] Marshall, H. E., and Stamler, J. S. (2001) Inhibition of NF-kappa B by S-nitrosylation *Biochemistry* **40,** 1688-93.

[96] Nemoto, T., Shimma, N., Horie, S., Saito, T., Okuma, Y., Nomura, Y., and Murayama, T. (2003) Involvement of the system L amino acid transporter on uptake of S-nitroso-L-cysteine, an endogenous S-nitrosothiol, in PC12 cells *Eur J Pharmacol* **458,** 17-24.

[97] Kerwin, J. F., Jr., Lancaster, J. R., Jr., and Feldman, P. L. (1995) Nitric oxide: a new paradigm for second messengers *J Med Chem* **38,** 4343-62.

[98] Hong, S. H., and Maret, W. (2003) A fluorescence resonance energy transfer sensor for the beta-domain of metallothionein *Proc Natl Acad Sci U S A* **100,** 2255-60.

[99] Chen, Y., Irie, Y., Keung, W. M., and Maret, W. (2002) S-nitrosothiols react preferentially with zinc thiolate clusters of metallothionein III through transnitrosation *Biochemistry* **41,** 8360-7.

[100] Jiang, L. J., Vasak, M., Vallee, B. L., and Maret, W. (2000) Zinc transfer potentials of the alpha - and beta-clusters of metallothionein are affected by domain interactions in the whole molecule *Proc Natl Acad Sci U S A* **97,** 2503-8.

[101] Schrammel, A., Behrends, S., Schmidt, K., Koesling, D., and Mayer, B. (1996) Characterization of 1H-[1,2,4]oxadiazolo[4,3-a]quinoxalin-1-one as a heme-site inhibitor of nitric oxide-sensitive guanylyl cyclase *Mol Pharmacol* **50,** 1-5.

[102] Griffiths, C., Wykes, V., Bellamy, T. C., and Garthwaite, J. (2003) A new and simple method for delivering clamped nitric oxide concentrations in the physiological range: application to activation of guanylyl cyclase-coupled nitric oxide receptors *Mol Pharmacol* **64,** 1349-56.